Journal of Mathematical Chemistry (2023) 61:777–804
https://doi.org/10.1007/s10910-022-01426-8

ORIGINAL PAPER

High-energy two-electron transfer in ion-atom collisions

Dževad Belkić[1,2]

Received: 20 October 2022 / Accepted: 20 November 2022 / Published online: 22 December 2022

Abstract
Two-electron transfer by fast heavy nuclei from heliumlike targets is studied. A detailed sequence of comprehensive computations is carried out in a large keV–MeV range of the projectile energies. This set is illustrated with total cross sections for double capture by alpha particles from helium atoms using several frequently applied four-body quantum-mechanical distorted wave models with the correct boundary conditions. The sensitivity of the obtained total cross sections is examined for different choices of the bound and continuum states. Especially at high energies, the influence of the compactness of the bound states is investigated by reference to the mechanism of the velocity matching kinematic double electron capture. Also considered is the dependence of these cross sections on the electronic screening of the projectile and the target nuclear charges in the bound and continuum states. The impact of this electronic shielding on total cross sections is assessed by reference to the corresponding bare nuclear charges in the bound and continuum states. Relative to all the available experimental data (100–6000 keV), the found striking model-dependence implies that two-electron transfer is sharply different from the associated one-electron transfer involving the same colliding particles.

Keywords Double charge exchange · Correct boundary conditions · Distorted waves

1 Introduction

We analyze double electron capture by a heavy nucleus of charge Z_P from a heliumlike target of nuclear charge Z_T. Intermediate and high impact energies are considered by applying several frequently used quantum-mechanical distorted wave methods with the correct boundary conditions. The concept of the correct boundary conditions for

✉ Dževad Belkić
Dzevad.Belkic@ki.se

1 Department of Oncology-Pathology, Karolinska Institute, P.O. Box 260, 171 76 Stockholm, Sweden

2 Medical Radiation Physics and Nuclear Medicine, Karolinska University Hospital, P.O. Box 260, 171 76 Stockholm, Sweden

double capture [1–3] is the same as for single capture [4]. Yet, in practice, most of the past applications of the customary distorted wave methods met with some huge surprises when passing from single to double capture, irrespective of whether the correct boundary conditions are fulfilled or disregarded.

In principle, vastly different choices of distorted waves are allowed under the provision that they are consistent with the distorting perturbation potentials and the correct asymptotic behaviors of the corresponding total scattering wave functions. Such choices can yield symmetric or asymmetric distorted wave methods. Symmetric methods do not need to separate the treatments of the homo-nuclear ($Z_P = Z_T$) and hetero-nuclear ($Z_P \neq Z_T$) collisions. On the other hand, for asymmetric methods, care should be exercised to select the physically appropriate variant (with the post or the prior interactions) depending on the ratio of the incident and target nuclear charges.

Given this constrained freedom of choices of distorted waves, a number of four-body (4B) methods have been introduced for single and double capture collisions. Some of the most frequently utilized theories are 'the boundary-corrected first Born' (CB1-4B) [5, 6], 'the continuum distorted wave' (CDW-4B) [7, 8], 'the boundary-corrected continuum intermediate state' (BCIS-4B) [9], the Born distorted wave (BDW-4B) [10, 11] and 'the continuum distorted wave - eikonal initial state' (CDW-EIS-4B) [12] methods. The BCIS-4B and BDW-4B methods use the CB1-4B method in one channel and the CDW-4B method in the other channel.

As to single charge-exchange, abundant experience with heliumlike and multi-electron targets demonstrated that these distorted wave methods systematically agree very well or excellently with measurements. Moreover, all the mentioned methods are in reasonably good mutual agreement for total cross sections within a common validity domain $E(\text{keV/amu}) \geq 80 \max\{I_i, I_f\}$, where I_i and I_f are the initial- and final-state ionization potentials, respectively [4].

By reference to virtually all the existing experimental data on total cross sections, the three-body boundary-corrected first Born (CB1-3B) method [4] for single capture by heavy nuclei from hydrogenlike and multi-electron targets emerged as ultimately the most successful first-order theory over a wide keV-MeV energy interval [13, 14]. Moreover, for single capture, the three-body second-order theories, e.g. the CDW-3B, CDW-EIS-3B, BCIS-3B and BDW-3B methods are also successful in providing reliable total cross sections at intermediate and high energies [15–17].

Some unexpected surprises were encountered in double capture by heavy nuclei from heliumlike targets. Namely, for such more complex collisions, no distorted wave method met with success uniformly throughout their anticipated validity domain of impact energies. For instance, in asymmetric double capture by protons from helium, $H^+ + He(1s^2) \rightarrow H^-(1s^2) + He^{2+}$, the CDW-4B method was in excellent agreement with the experimental data above about 100 keV [7, 8].

However, for symmetric double capture by $\alpha-$particles from helium, $He^{2+} + He(1s^2) \rightarrow He(1s^2) + He^{2+}$, the CDW-4B method underestimated the experimental data by a factor of 2-10 at $250 \leq E \leq 3000$ keV [10, 11]. For this collision, at the same energies, the CDW-EIS-4B method suffered a complete breakdown by underestimating the measured total cross sections by 3-4 orders of magnitudes [12]. Moreover, for the same scattering, the CB1-4B method had a drastic failure above 2000 keV/amu through overestimation of the experimental data by 2–3 orders of magnitude [1–3]. As

such, in this process, the first- and second-order methods predicted the diametrically opposite behaviors of total cross sections as a function of impact energy. Specifically, total cross sections in the CB1-4B method are too high, whereas those in the CDW-4B and CDW-EIS-4B methods are too low relative to the corresponding findings from the measurements.

On the other hand, for this identical double capture problem, reproduction of the experimental data by the BCIS-4B and BDW-4B methods is either within a factor of 2 or excellent below or above 1000 keV, respectively. It then follows that double capture is extremely sensitive to different choices of distorted waves and distorting potentials, even when relying exclusively upon the methods with the correct boundary conditions.

This is all the more unusual, especially in comparison to a relatively mild sensitivity of single capture to vastly different selections of distorted waves and distorting potentials. It should be emphasized, however, that the requirement for the orbital compactness in double capture is very demanding. In double capture, the two electrons from the target must be at nearly the same place at about the same time to be simultaneously captured by the projectile.

A strong model-dependence of theoretical descriptions of double capture might partially be attributed to the 'multiplicative effect' of the electronic distortions included either in one (BCIS-4B, BDW-4B) or both (CDW-4B, CDW-EIS-4B) channels of scattering. Therein, this effect is manifested in the appearance of the product of the two electronic Coulomb wave functions (or their eikonal asymptotes) in the entrance or exit channels or both. In single capture, the same mentioned methods contain only one electronic Coulomb distortion (or its eikonal asymptote) per channel. The implication is that e.g. some linear errors in distorted wave models for single capture could be exacerbated and become quadratic (or even of a higher order) for double capture.

Given all the intertwined issues, it is difficult to assess the relative influence of various contributing factors to double capture by examining simultaneously several effects. Instead, it could be more insightful to examine separately some of the salient characteristics of double capture, as envisaged in the present study. We choose to focus on the Slater screening effect because of its direct influence on the critically important compactness of the initial and final bound state orbitals.

Our goal is broader, however, because of aiming to assess the role of the electronic shielding of the nuclear charges in both the bound and continuum states in the entrance and exit channels. To this end, three different settings are considered for the mentioned pivotal collision, $He^{2+} + He(1s^2) \rightarrow He(1s^2) + He^{2+}$, such as (i) bound and continuum states unscreened: $Z_{P,T} = 2$, (ii) bound states screened: $Z_{P,T}^{\text{eff}} = 1.6875$ and continuum states unscreened: $Z_{P,T} = 2$ as well as (iii) bound and continuum states screened: $Z_{P,T}^{\text{eff}} = 1.6875$.

The role of the addressed effects is evaluated by reference to all the experimental data from different measurements available at 100-6000 keV (Allison [18], Nikolaev *et al* [19], Pivovar *et al* [20], Berkner *et al* [21], McDaniel *et al* [22], DuBois [23], de Castro Faria *et al* [24], Schuch *et al* [25], Afrosimov *et al* [26]).

Atomic units will be used throughout unless otherwise stated.

2 Theory

We consider non-radiative, non-relativistic double electron capture by a heavy projectile nucleus P of incident velocity $\boldsymbol{v}$ from a heliumlike target (taken at rest), which has a heavy nucleus T. This process is schematized as follows:

$$Z_{\rm P} + (Z_{\rm T}; e_1, e_2)_i \longrightarrow (Z_{\rm P}; e_1, e_2)_f + Z_{\rm T} \quad \text{(Double capture)}, \tag{2.1}$$

where e_k is k th electron ($k = 1, 2$) and the parentheses indicate the bound states with the usual sets of the initial and final quantum numbers $\{i, f\}$, respectively. The charge and mass of nucleus K are denoted by $Z_{\rm K}$ and $M_{\rm K}$ (K=P, T), respectively. In the adopted atomic units, the electron mass m_e is $m_e = 1$. The reduced masses in the entrance and exit channels in process (2.1) are $\mu_i = M_{\rm P}(M_{\rm T} + 2)/M$ and $\mu_f = M_{\rm T}(M_{\rm P} + 2)/M$, respectively, with $M = M_{\rm P} + M_{\rm T} + 2$.

All the four particles $\{Z_{\rm P}, Z_{\rm T}, e_1, e_2\}$ in process (2.1) are viewed as being the active participants to the transition $i \to f$. Each of them is treated quantum-mechanically in the CB1-4B, CDW-4B, CDW-EIS-4B, BCIS-4B and BDW-4B methods. For the geometry of process (2.1), let $\boldsymbol{s}_k$ and $\boldsymbol{x}_k$ be the position vectors of the k th electron relative to P and T, respectively ($k = 1, 2$). Further, let $\boldsymbol{R}$ be the relative vector of $Z_{\rm P}$ with respect to $Z_{\rm T}$. For the relative motion of heavy particles, the quantities $\boldsymbol{r}_i$ and $\boldsymbol{r}_f$ are introduced as the position vectors of P and T with respect to the centers-of-masses of the atomic systems $(Z_{\rm T}; e_1, e_2)_i$ and $(Z_{\rm P}; e_1, e_2)_f$, respectively.

Vector $\boldsymbol{R}$ can be decomposed as $\boldsymbol{R} = \boldsymbol{\rho} + v\hat{\boldsymbol{Z}}$. Here, $\boldsymbol{\rho}$ is a two-dimensional vectorial component of $\boldsymbol{R}$ in the scattering plane (XOY) and $\hat{\boldsymbol{Z}}$ is the unit vector of the Z-axis. Vector $\boldsymbol{v}$ is taken to be along the Z-axis, so that $\boldsymbol{\rho} \cdot \boldsymbol{v} = 0$.

The initial and final wave vectors are labeled by $\boldsymbol{k}_i = \mu_i \boldsymbol{v}_i$ and $\boldsymbol{k}_f = \mu_f \boldsymbol{v}_f$, where $\boldsymbol{v}_i$ and $\boldsymbol{v}_f$ are the velocities of the incident and scattered projectile, respectively. In the heavy mass limit, forward scattering dominates and, moreover, with the target assumed to be at rest, it follows that $\boldsymbol{v}_f \approx \boldsymbol{v}_i \equiv \boldsymbol{v}$. We take $\boldsymbol{k}_i$ to be the momentum vector of P with respect to $(Z_{\rm T}; e_1, e_2)_i$, whereas $\boldsymbol{k}_f$ is the momentum vector of $(Z_{\rm P}; e_1, e_2)_f$ relative to T. For heavy particle collisions, the standard mass limits $1/M_{\rm P,T} \ll 1$ in process (2.1) will consistently be used throughout.

We will also discuss non-radiative, non-relativistic single electron capture for the same entrance channel as in process (2.1), but with a different exit channel, as symbolized by:

$$Z_{\rm P} + (Z_{\rm T}; e_1, e_2)_i \longrightarrow (Z_{\rm P}, e_1)_{f_1} + (Z_{\rm T}, e_2)_{f_2} \quad \text{(Single capture)}, \tag{2.2}$$

where $\{f_1, f_2\}$ is the standard set of the final quantum numbers of the two hydrogenlike atomic systems.

As elaborated in Ref. [2], the CB1-4B, CDW-4B, CDW-EIS-4B, BCIS-4B and BDW-4B methods have the following exponential term in common:

$$\mathcal{D} \equiv \mathrm{e}^{i\boldsymbol{k}_i\cdot\boldsymbol{r}_i + i\boldsymbol{k}_f\cdot\boldsymbol{r}_f} = \mathrm{e}^{i\boldsymbol{\alpha}\cdot(\boldsymbol{s}_1+\boldsymbol{s}_2) + i\boldsymbol{\beta}\cdot(\boldsymbol{x}_1+\boldsymbol{x}_2)}, \tag{2.3}$$

where $\boldsymbol{\alpha}$ and $\boldsymbol{\beta}$ are the momentum transfer vectors given by the relations[1]

$$\boldsymbol{\alpha} = \frac{\boldsymbol{\eta} - v^{+}\hat{\boldsymbol{v}}}{2},\ \boldsymbol{\beta} = -\frac{\boldsymbol{\eta} + v^{-}\hat{\boldsymbol{v}}}{2},\ \boldsymbol{\alpha} + \boldsymbol{\beta} = -\boldsymbol{v},\ v^{\pm} = v \pm \frac{\epsilon_f^{\mathrm{P}} - \epsilon_i^{\mathrm{T}}}{v}. \tag{2.4}$$

Here, $\boldsymbol{\eta}$ is the vector of the transverse momentum transfer with the property $\boldsymbol{\eta} \cdot \boldsymbol{v} = 0$. Further, ϵ_i^{T} and ϵ_f^{P} are the binding energies associated with the initial and final bound-state wave functions $\varphi_i(\boldsymbol{x}_1, \boldsymbol{x}_2)$ and $\varphi_f(\boldsymbol{s}_1, \boldsymbol{s}_2)$ of the two-electron systems $(Z_{\mathrm{T}}; e_1, e_2)_i$ and $(Z_{\mathrm{P}}; e_1, e_2)_f$ in the entrance and exit channels of process (2.1), respectively.

We will now list the working formulae for the transition amplitudes in the CB1-4B, CDW-4B, CDW-EIS-4B, BCIS-4B and BDW-4B methods for double capture in process (2.1). The prior and post forms of the transition amplitudes are denoted by the standard symbols T_{if}^{-} and T_{if}^{+}, respectively. There is no need to give any further details as they can be found in Ref. [2].

All the analyzed results will be for total cross sections alone. In the CB1-4B, CDW-4B, CDW-EIS-4B, BCIS-4B and BDW-4B methods, total cross sections do not depend on the internuclear potential nor on any other $\rho-$dependent phase stemming from the relative motion of heavy scattering aggregates interacting through the Coulomb potentials [2]. This should be the case with any other theory which accounts for the internuclear potential exactly in the heavy mass limit and obeys the correct Coulomb boundary conditions.

Therefore, the $\rho-$dependent phases will be omitted throughout. If differential cross sections are needed, these phases must be included and they can be taken from Ref. [2]. For differential cross sections in the CDW-4B and CDW-EIS-4B methods for any value of $Z_{\mathrm{P,T}}$, the difficult Bessel-Fourier numerical quadrature is employed with the highly oscillatory functions. Advantageously, this is completely unnecessary in the BCIS-4B and BDW-4B methods for $Z_{\mathrm{P}} = 2$ or $Z_{\mathrm{T}} = 2$ in which case the differential cross sections are directly proportional to $|T_{if}^{\pm}|^2$ [2].

2.1 The CB1-4B method (prior and post)

$$T_{if}^{(\mathrm{CB1-4B})-}(\boldsymbol{\eta}) = \iiint \mathrm{d}\boldsymbol{x}_1 \mathrm{d}\boldsymbol{x}_2 \mathrm{d}\boldsymbol{R}\, (vR - \boldsymbol{v}\cdot\boldsymbol{R})^{2i\xi} \mathcal{D}\mathcal{F}_{if}^{-}, \tag{2.5}$$

$$T_{if}^{(\mathrm{CB1-4B})+}(\boldsymbol{\eta}) = \iiint \mathrm{d}\boldsymbol{x}_1 \mathrm{d}\boldsymbol{x}_2 \mathrm{d}\boldsymbol{R}\, (vR + \boldsymbol{v}\cdot\boldsymbol{R})^{-2i\xi} \mathcal{D}\mathcal{F}_{if}^{+}, \tag{2.6}$$

$$\mathcal{F}_{if}^{-} = \varphi_f^{*}(\boldsymbol{s}_1, \boldsymbol{s}_2) \left[Z_{\mathrm{P}} \left(\frac{2}{R} - \frac{1}{s_1} - \frac{1}{s_2} \right) \right] \varphi_i(\boldsymbol{x}_1, \boldsymbol{x}_2), \tag{2.7}$$

$$\mathcal{F}_{if}^{+} = \varphi_f^{*}(\boldsymbol{s}_1, \boldsymbol{s}_2) \left[Z_{\mathrm{T}} \left(\frac{2}{R} - \frac{1}{x_1} - \frac{1}{x_2} \right) \right] \varphi_i(\boldsymbol{x}_1, \boldsymbol{x}_2), \tag{2.8}$$

$$\xi = \frac{Z_{\mathrm{T}} - Z_{\mathrm{P}}}{v}. \tag{2.9}$$

[1] There are some misprints in Refs. [2]: and they are corrected here. Therein, on p. 9: $2\boldsymbol{\alpha}\cdot(\boldsymbol{s}_1+\boldsymbol{s}_2)+2\boldsymbol{\beta}\cdot(\boldsymbol{x}_1+\boldsymbol{x}_2)$ should read $\boldsymbol{\alpha}\cdot(\boldsymbol{s}_1+\boldsymbol{s}_2)+\boldsymbol{\beta}\cdot(\boldsymbol{x}_1+\boldsymbol{x}_2)$ (number 2 removed). Further, on p. 24 in Ref. [2]: $\boldsymbol{2\alpha} = \boldsymbol{\eta} - v^{+}\hat{\boldsymbol{v}}$ and $\boldsymbol{2\beta} = -\boldsymbol{\eta} - v^{-}\hat{\boldsymbol{v}}$ should read $2\boldsymbol{\alpha} = \boldsymbol{\eta} - v^{+}\hat{\boldsymbol{v}}$ and $2\boldsymbol{\beta} = -\boldsymbol{\eta} - v^{-}\hat{\boldsymbol{v}}$, respectively (no bolding of number 2, but α and β are bolded).

2.2 The CDW-4B method (prior and post)

$$T_{if}^{(\mathrm{CDW-4B})-}(\boldsymbol{\eta}) = -[N^{\star}(\nu_{\mathrm{P}})N(\nu_{\mathrm{T}})]^2 \iiint \mathrm{d}\boldsymbol{x}_1 \mathrm{d}\boldsymbol{x}_2 \mathrm{d}\boldsymbol{R} \times \prod_{k=1}^{2} {}_1F_1(i\nu_{\mathrm{T}}, 1, ivx_k + i\boldsymbol{v}\cdot\boldsymbol{x}_k)\mathcal{D}\mathcal{G}_{if}^{-}, \tag{2.10}$$

$$T_{if}^{(\mathrm{CDW-4B})+}(\boldsymbol{\eta}) = -[N^{\star}(\nu_{\mathrm{P}})N(\nu_{\mathrm{T}})]^2 \iiint \mathrm{d}\boldsymbol{s}_1 \mathrm{d}\boldsymbol{s}_2 \mathrm{d}\boldsymbol{R} \times \prod_{k=1}^{2} {}_1F_1(i\nu_{\mathrm{P}}, 1, ivs_k + i\boldsymbol{v}\cdot\boldsymbol{s}_k)\mathcal{D}\mathcal{G}_{if}^{+}, \tag{2.11}$$

$$\mathcal{G}_{if}^{-} = \varphi_f^*(\boldsymbol{s}_1, \boldsymbol{s}_2)\left\{ {}_1F_1(i\nu_{\mathrm{P}}, 1, ivs_2 + i\boldsymbol{v}\cdot\boldsymbol{s}_2)\nabla_{x_1}\varphi_i(\boldsymbol{x}_1, \boldsymbol{x}_2)\cdot\nabla_{s_1}\, {}_1F_1(i\nu_{\mathrm{P}}, 1, ivs_1 + i\boldsymbol{v}\cdot\boldsymbol{s}_1) + {}_1F_1(i\nu_{\mathrm{P}}, 1, ivs_1 + i\boldsymbol{v}\cdot\boldsymbol{s}_1)\nabla_{x_2}\varphi_i(\boldsymbol{x}_1, \boldsymbol{x}_2)\cdot\nabla_{s_2}\, {}_1F_1(i\nu_{\mathrm{P}}, 1, ivs_2 + i\boldsymbol{v}\cdot\boldsymbol{s}_2)\right\}, \tag{2.12}$$

$$\mathcal{G}_{if}^{+} = \varphi_i(\boldsymbol{x}_1, \boldsymbol{x}_2)\left\{ {}_1F_1(i\nu_{\mathrm{T}}, 1, ivx_2 + i\boldsymbol{v}\cdot\boldsymbol{x}_2)\nabla_{s_1}\varphi_f^*(\boldsymbol{s}_1, \boldsymbol{s}_2)\cdot\nabla_{x_1}\, {}_1F_1(i\nu_{\mathrm{T}}, 1, ivx_1 + i\boldsymbol{v}\cdot\boldsymbol{x}_1) + {}_1F_1(i\nu_{\mathrm{T}}, 1, ivx_1 + i\boldsymbol{v}\cdot\boldsymbol{x}_1)\nabla_{s_2}\varphi_f^*(\boldsymbol{s}_1, \boldsymbol{s}_2)\cdot\nabla_{x_2}\, {}_1F_1(i\nu_{\mathrm{T}}, 1, ivx_2 + i\boldsymbol{v}\cdot\boldsymbol{x}_2)\right\}, \tag{2.13}$$

$$N^{\pm}(\nu_{\mathrm{K}}) = \mathrm{e}^{\pi\nu_{\mathrm{K}}/2}\Gamma(1 \pm i\nu_{\mathrm{K}}), \;\; \nu_{\mathrm{K}} = \frac{Z_{\mathrm{K}}}{v} \;\; (\mathrm{K} = \mathrm{P}, \mathrm{T}). \tag{2.14}$$

Here, the standard symbols ${}_1F_1(a, b, z)$ and $\Gamma(z)$ denote the Kummer confluent hypergeometric function and the Euler gamma function, respectively. Moreover, ν_{K} is the usual notation for the Sommerfeld parameter.

2.3 The CDW-EIS-4B method (post)

$$T_{if}^{(\mathrm{CDW-EIS-4B})+}(\boldsymbol{\eta}) = -[N(\nu_{\mathrm{T}})]^2 \iiint \mathrm{d}\boldsymbol{s}_1 \mathrm{d}\boldsymbol{s}_2 \mathrm{d}\boldsymbol{R} \prod_{k=1}^{2} (vs_k + \boldsymbol{v}\cdot\boldsymbol{s}_k)^{-i\nu_{\mathrm{P}}}\mathcal{D}\mathcal{G}_{if}^{+}. \tag{2.15}$$

2.4 The BCIS-4B method (prior and post)

$$T_{if}^{(\mathrm{BCIS-4B})-}(\boldsymbol{\eta}) = -[N(\nu_{\mathrm{T}})]^2 \iiint \mathrm{d}\boldsymbol{x}_1 \mathrm{d}\boldsymbol{x}_2 \mathrm{d}\boldsymbol{R}(vR - \boldsymbol{v}\cdot\boldsymbol{R})^{-2i\nu_{\mathrm{P}}}\mathcal{D}\mathcal{H}_{if}^{-}, \tag{2.16}$$

$$T_{if}^{(\mathrm{BCIS-4B})+}(\boldsymbol{\eta}) = -[N^{\star}(\nu_{\mathrm{P}})]^2 \iiint \mathrm{d}\boldsymbol{s}_1 \mathrm{d}\boldsymbol{s}_2 \mathrm{d}\boldsymbol{R}(vR + \boldsymbol{v}\cdot\boldsymbol{R})^{-2i\nu_{\mathrm{T}}}\mathcal{D}\mathcal{H}_{if}^{+}, \tag{2.17}$$

$$\mathcal{H}_{if}^{-} = \varphi_f^*(\boldsymbol{s}_1, \boldsymbol{s}_2)\left[Z_{\mathrm{P}}\left(\frac{2}{R} - \frac{1}{s_1} - \frac{1}{s_2}\right)\right]\varphi_i(\boldsymbol{x}_1, \boldsymbol{x}_2) \times {}_1F_1(i\nu_{\mathrm{T}}, 1, ivx_1 + i\boldsymbol{v}\cdot\boldsymbol{x}_1)\, {}_1F_1(i\nu_{\mathrm{T}}, 1, ivx_2 + i\boldsymbol{v}\cdot\boldsymbol{x}_2), \tag{2.18}$$

$$\mathcal{H}_{if}^{+} = \varphi_f^*(\boldsymbol{s}_1, \boldsymbol{s}_2)\left[Z_{\mathrm{T}}\left(\frac{2}{R} - \frac{1}{x_1} - \frac{1}{x_2}\right)\right]\varphi_i(\boldsymbol{x}_1, \boldsymbol{x}_2) \times {}_1F_1(i\nu_{\mathrm{P}}, 1, ivs_1 + i\boldsymbol{v}\cdot\boldsymbol{s}_1)\, {}_1F_1(i\nu_{\mathrm{P}}, 1, ivs_2 + i\boldsymbol{v}\cdot\boldsymbol{s}_2). \tag{2.19}$$

2.5 The BDW-4B method (prior and post)

$$T_{if}^{(\mathrm{BDW-4B})-}(\boldsymbol{\eta}) = -[N^{\star}(\nu_{\mathrm{P}})]^2 \iiint \mathrm{d}\boldsymbol{x}_1 \mathrm{d}\boldsymbol{x}_2 \mathrm{d}\boldsymbol{R}\, (vR + \boldsymbol{v}\cdot\boldsymbol{R})^{-2i\nu_{\mathrm{T}}} \mathcal{DG}_{if}^{-}, \quad (2.20)$$

$$T_{if}^{(\mathrm{BDW-4B})+}(\boldsymbol{\eta}) = -[N(\nu_{\mathrm{T}})]^2 \iiint \mathrm{d}\boldsymbol{s}_1 \mathrm{d}\boldsymbol{s}_2 \mathrm{d}\boldsymbol{R}\, (vR - \boldsymbol{v}\cdot\boldsymbol{R})^{-2i\nu_{\mathrm{P}}} \mathcal{DG}_{if}^{+}. \quad (2.21)$$

2.6 Common aspects on numerical computations in all the methods

The defining nine-dimensional integrals in all the just listed expressions for the transition amplitudes are reduced to certain lower dimensions by analytical means. This is done using the Fourier integral transform, followed by the techniques of Feynman, Nordsieck and Lewis [7, 9]. Depending on the analyzed distorted wave method, the remaining two- to four-dimensional integrals in $T_{if}^{\pm}$ must be computed by numerical quadratures. Thus, in the CB1-4B method, the transition amplitudes are computed by two- or three-dimensional numerical quadratures [5, 6]. For the CDW-4B, CDW-EIS-4B, BCIS-4B and BDW-4B methods, the number of numerical quadratures in $T_{if}^{\pm}$ is three [7–10, 12]. Alternatively, the transition amplitude in the BCIS-4B and BDW-4B methods can be computed by four-dimensional numerical quadratures [9, 10]. In these two latter methods, computations by three and four-dimensional numerical quadratures in $T_{if}^{\pm}$ are carried out at several energies to confirm the same accuracy of the obtained results.

The prior Q_{if}^{-} and post Q_{if}^{+} total cross sections are computed from the usual expressions:

$$Q_{if}^{\mp}(a_0^2) = \int_0^{\infty} \mathrm{d}\eta \left| \frac{T_{if}^{\mp}(\boldsymbol{\eta})}{2\pi v} \right|^2, \quad (2.22)$$

where a_0 is the Bohr radius. Using the relation $\pi a_0^2 = 8.797356 \times 10^{-17}\mathrm{cm}^2$, these cross sections are expressed in cm^2 in all the plotted graphs on Figs. 1-10. For the ground-to-ground state transition, $T_{if}^{\mp}(\boldsymbol{\eta})$ do not depend on ϕ_η, i.e $T_{if}^{\mp}(\eta) = T_{if}^{\mp}(\boldsymbol{\eta})$. The ensuing result of the integration over ϕ_η in (2.22) is 2π. Thus, total cross sections $Q_{if}^{\mp}$ are computed by three- to at most five-dimensional numerical quadratures, depending on the employed distorted wave method (as well as on the prior procedure in the partial analytical reduction of $T_{if}^{\mp}$). Using the CDW-4B, BCIS-4B, BDW-4B and CB1-4B methods for the symmetric case $Z_{\mathrm{T}} = Z_{\mathrm{P}} = 2$ of process (2.1), i.e. $^4\mathrm{He}^{2+} + {}^4\mathrm{He}(1s^2) \rightarrow {}^4\mathrm{He}(1s^2) + {}^4\mathrm{He}^{2+}$, our computations explicitly confirmed that there is no post-prior discrepancy, as expected.

3 Results

In the illustrations, the general double capture process (2.1) is specified as the symmetric homo-nuclear collisions ($Z_{\mathrm{T}} = Z_{\mathrm{P}} = 2$) for the ground-to-ground state transition

(in computations):

$$^4\mathrm{He}^{2+} + {}^4\mathrm{He}(1\mathrm{s}^2) \longrightarrow {}^4\mathrm{He}(1\mathrm{s}^2) + {}^4\mathrm{He}^{2+} \quad \text{(Double capture)}, \tag{3.1}$$

as well as for any final state (in measurements)

$$^4\mathrm{He}^{2+} + {}^4\mathrm{He}(1s^2) \longrightarrow {}^4\mathrm{He}(\Sigma) + {}^4\mathrm{He}^{2+} \quad \text{(Double capture)}. \tag{3.2}$$

Moreover, regarding the general single capture process (2.2), we shall also refer to the homo-nuclear case $Z_\mathrm{T} = Z_\mathrm{P} = 2$ by using only the ground states $i = 1s^2$ as well as $f_1 = 1s$ and $f_2 = 1s$:

$$^4\mathrm{He}^{2+} + {}^4\mathrm{He}(1s^2) \longrightarrow {}^4\mathrm{He}^{+}(1s) + {}^4\mathrm{He}^{+}(1s) \quad \text{(Single capture)}. \tag{3.3}$$

We will start by examining the sensitivity of the computed cross sections to several initial φ_i and final φ_f heliumlike ground-state wave functions. The selected wave functions with one, two, three and four parameters are due to Hylleraas [27], Silverman *et al* [28], Green *et al* [29] and Löwdin [30], respectively.

Throughout, the same given type of the ground-state wave functions centered on Z_T and Z_P is used for φ_i and φ_f, respectively. For instance, the same type of the ground-state helium wave functions $\varphi_i(\boldsymbol{x}_1, \boldsymbol{x}_2)$ and $\varphi_f(\boldsymbol{s}_1, \boldsymbol{s}_2)$ of Hylleraas [27] is employed for $(Z_\mathrm{T}, 2e)_{i=1s^2}$ and $(Z_\mathrm{P}, 2e)_{f=1s^2}$ in the entrance and exit channel, respectively. The like procedure also applies to each of the other three types of the quoted ground-state helium wave functions taken one at a time.

The heliumlike wave functions from Refs. [27–30] include only the radial electron-electron correlations. The extent of this static correlation differs from one function to another. Thus, for the most frequently used two-parameter ground-state helium wave function of Silverman *et al* [28], the included radial correlations are very high (up to about 95%).

For brevity, regarding the choice of the ground-state wave functions, the sensitivity test is carried out for the CDW-4B method alone. The results for process (3.1) are shown in Figs. 1 and 2. Figure 1 has four panels each of which compares two wave functions at a time. The results for the one-parameter wave function [27] are on every panel (a-d). The results for the two [28], three [29] and four [30] parameter wave functions are on panels (a), (b) and (c), respectively. The cross sections for all the four ground-state wave functions [27–30] are summarized on panel (d). In panels (a-d), the impact energy and cross sections vary within $10^2 - 10^4$ keV and $10^{-28} - 10^{-15}$ cm^2, respectively.

At least for this very large span of some 13 orders of magnitudes on the ordinates, the cross sections are visually observed to be not very much dependent on the choice of the helium wave functions. This is also partially reflected on panel (d) of Fig. 1, where the most notable dispersion of the curves occurs at high impact energies.

Figure 2 is an enlarged version of Fig. 1d. In Fig. 2, the increased disparity among the four bottom curves for double capture in process (3.1) with the augmented impact energy is more visible than in Fig. 1d. In Fig. 2, at high energies, the larger total cross sections are seen for the wave function of Silverman *et al* [28] compared to those

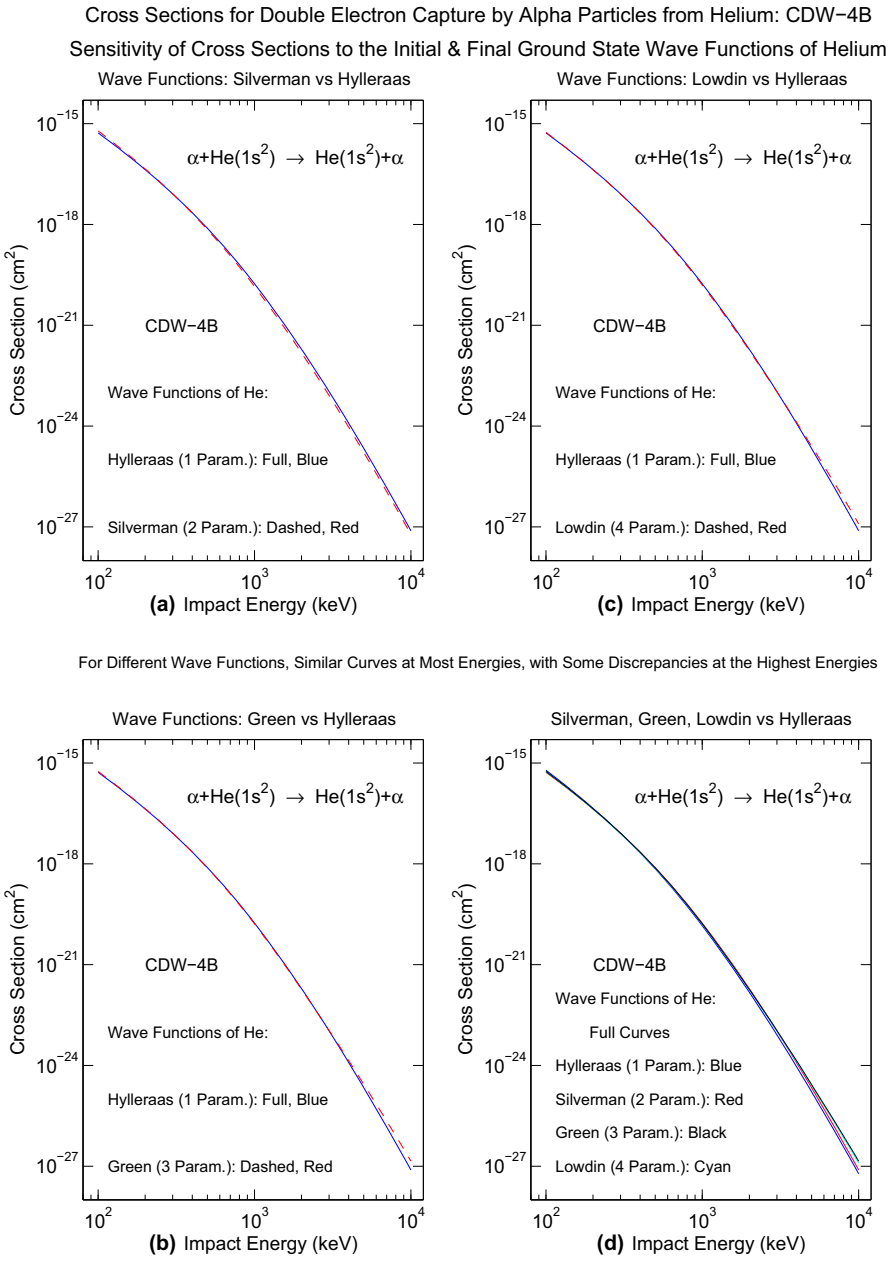

Fig. 1 Total cross sections $Q(\mathrm{cm}^2)$ as a function of impact energy $E(\mathrm{keV})$ for double capture (3.1). Sensitivity of the results from the CDW-4B method relative to the choice of the ground-state wave functions with 1-4 parameters. The electronic full continuum Coulomb wave functions are centered on the bare nuclear charges $Z_{\mathrm{P,T}}$. Each panel compares two ground-state wave functions at a time. The results for the one-parameter wave function [27], are on every panel (a-d). The results for the two [28], three [29] and four [30] parameter wave functions are on panels (a), (b) and (c), respectively. All the four results are summarized on panel (d). For details, see the main text (color online)

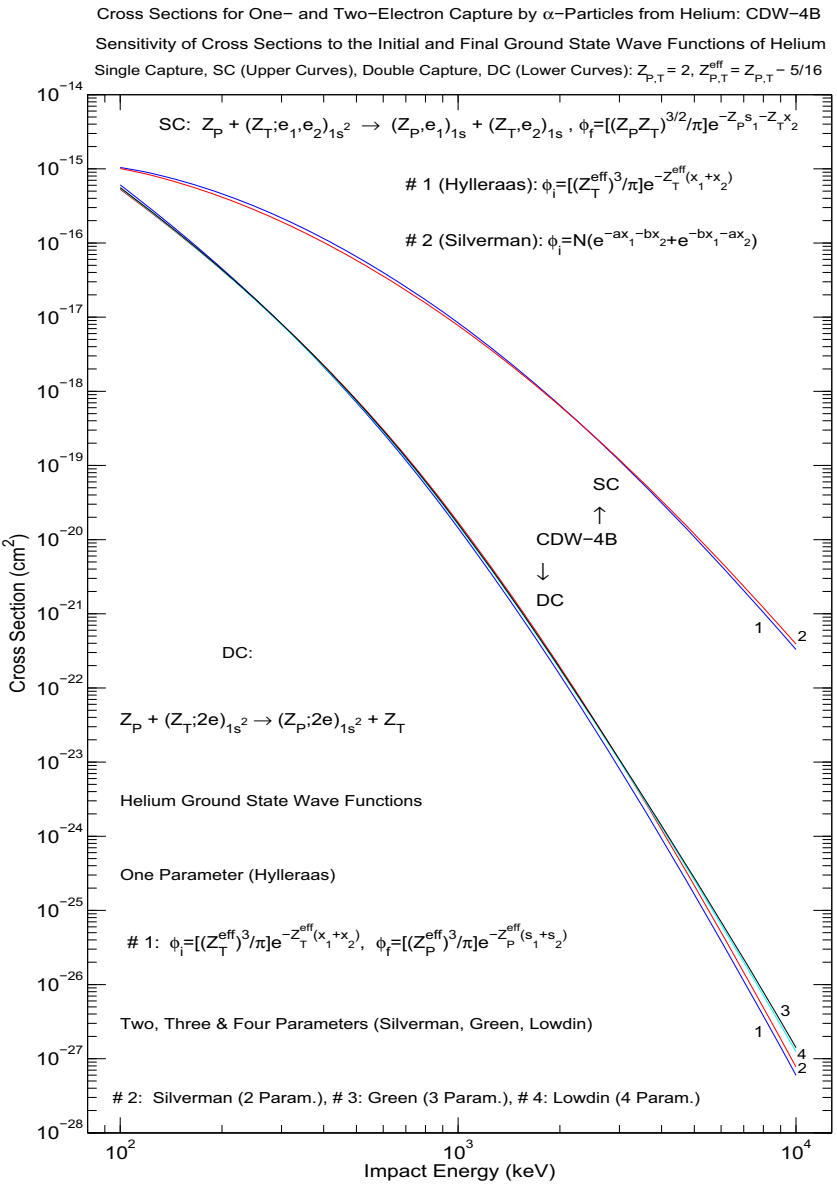

Fig. 2 Total cross sections $Q(\text{cm}^2)$ as a function of impact energy $E(\text{keV})$ for single and double capture. Sensitivity of the results from the CDW-4B method relative to the choice of the ground-state wave functions with 1-4 parameters. The electronic full continuum Coulomb wave functions are centered on the bare nuclear charges $Z_{P,T} = 2$ for double capture (3.1) and on $\{Z_P = 2,\ Z_T - 1 = 1\}$ for single capture (3.3). Curves denoted by 1-4 refer to the ground-state helium wave functions with 1-4 parameters [27–30], respectively. For details, see the main text (color online)

of Hylleraas [27]. This is attributed to the mentioned strong electron-electron radial correlations in the ground-state helium wave function of Silverman *et al* [28]. On the other hand, Fig. 2 shows that at intermediate energies (100-800 keV), the curves for four different helium ground-state wave functions are very close to each other. Such an observation coheres with the well-known fact that in ion-atom collisions, the inter-electronic correlations play an important role at low and high, but not at intermediate energies.

Further, it is instructive to juxtapose the total cross sections from the CDW-4B method for double and single capture in processes (3.1) and (3.3), corresponding to the upper and lower traces in Fig. 2, respectively. The displayed results for single capture in the CDW-4B method [31] refer to the ground-state helium wave functions from Refs. [27, 28]. For these two wave functions, the relative difference between the corresponding curves ('1' and '2') for single capture (upper plot) is seen in Fig. 2 to be very similar to that with the associated curves '1' and '2' for double capture (lower plot).

In the subsequent analysis, for simplicity, we shall employ only the one-parameter ground-state helium wave functions. Specifically, besides the one-parameter wave function of Hylleraas [27], use will also be made of the product of the two hydrogenlike wave functions, each centered on the same bare nuclear charge, $Z_{\rm T} = 2$ (entrance channel) and $Z_{\rm P} = 2$ (exit channel). As such, the difference between this one-parameter 'hydrogenic model' and the one-parameter 'Hylleraas model' is that the former and the latter treatments are based on the unscreened ($Z_{\rm P,T} = 2$) and screened ($Z^{\rm eff}_{\rm P,T} = 1.6875$), nuclear charges, respectively.

There is a physical difference between the Hamiltonians for the heliumlike eigenvalue problems in the Hylleraas and hydrogenic models. Of course, it is because of the presence of $1/r_{12}$ in the heliumlike ground-state electronic Hamiltonian that the minimal variational binding energy is obtained for $Z^{\rm eff}_{\rm P,T} = Z_{\rm P,T} - 5/16$ in the Hylleraas model. By contrast, the pure hydrogenic model has $1/r_{12} = 0$ from the onset. As such, the Hylleraas model is correlated (albeit crudely), whereas the hydrogenic model is completely uncorrelated.

It is then important to assess the sensitivity of total cross sections to the screening effect in which the electrons shield the bare nuclear charges $Z_{\rm P,T} = 2$. Such a shielding effect in the CDW-4B method can take place in either the bound or continuum or both states in each of the two channels. An approach, which is deemed optimal is to consider the influence of the shielding effect first separately on the bound and continuum states. Subsequently, a combined effect can be analyzed for the bound and continuum states considered in concert.

With this goal, Fig. 3 shows the total cross sections from the CDW-4B method for ground-to-ground-state single capture (upper trace) and double capture (lower trace) by alpha particles from helium targets. Therein, the full and dashed curves denoted by $1_{\rm Hyll}$ and $1_{\rm Hydr}$ refer to the one-parameter ground-state helium wave functions with and without screening, i.e. for the nuclear charges $Z^{\rm eff}_{\rm P,T} = 1.6875$ (the Hylleraas model) and $Z_{\rm P,T} = 2$ (the hydrogenic model), respectively.

In the lower plot, large differences exist between the curves $1_{\rm Hyll}$ and $1_{\rm Hydr}$. Namely, the cross section ratios $Q_{\rm Hydr}/Q_{\rm Hyll}$ for double capture vary within an order of magnitude as 1.57, 2.68 and 9.68 at 100, 1000 and 10000 keV, respectively. By comparison,

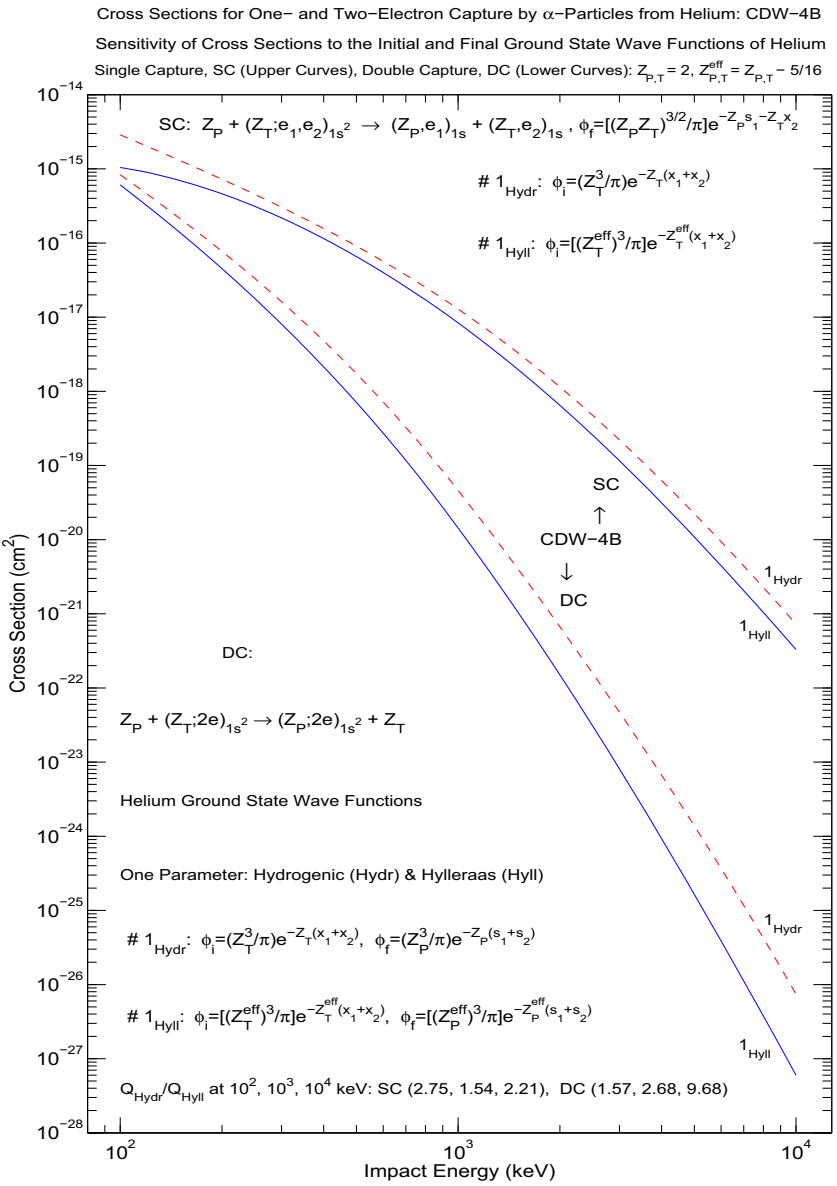

Fig. 3 Total cross sections $Q(\mathrm{cm}^2)$ as a function of impact energy $E(\mathrm{keV})$ for single and double capture. Sensitivity of the results from the CDW-4B method relative to the screening of the nuclear charges in the one-parameter ground-state wave functions. The electronic full continuum Coulomb wave functions are centered on the bare nuclear charges $Z_{\mathrm{P,T}} = 2$ for double capture (3.1) and on $\{Z_{\mathrm{P}} = 2,\ Z_{\mathrm{T}} - 1 = 1\}$ for single capture (3.3. The parameters in the exponentials of the screened and unscreened electronic orbitals from the helium ground state are $Z^{\mathrm{eff}}_{\mathrm{P,T}} = 1.6875$ and $Z_{\mathrm{P,T}} = 2$ for the Hylleraas [27] and hydrogenic models, as indicated near the drawn curves by the labels 1_{Hyll} and 1_{Hydr}, respectively. For details, see the main text (color online)

the corresponding cross section ratios $Q_{\mathrm{Hydr}}/Q_{\mathrm{Hyll}}$ for single capture are seen to change within a notably smaller factor (less than three) as 2.75, 1.54 and 2.21 at 100, 1000 and 10000 keV, respectively. In particular, e.g. at 10000 keV, the cross section ratio $Q_{\mathrm{Hydr}}/Q_{\mathrm{Hyll}}$ (unscreened vs. screened ground states) is about 4.38 times larger for double than for single capture ($9.68/2.21 \approx 4.38$). In Fig. 3, for both considered cases (the unscreened and screened ground-state wave functions), the CDW-4B method for double capture uses the two electronic full Coulomb wave functions per channel centered on the appropriate bare nuclear charges ($Z_{\mathrm{P,T}} = 2$). For single capture with both the unscreened and screened ground-state wave functions, the CDW-4B method employs two electronic full Coulomb wave functions altogether, one in the entrance and the other in the exit channel centered on $Z_{\mathrm{P}} = 2$ and $Z_{\mathrm{T}} - 1$, respectively.

There is a physical reason in Fig. 3 for having the curve 1_{Hydr} for the larger nuclear charge ($Z_{\mathrm{P,T}} = 2$, without screening in $\varphi_{i,f}$) as lying above the curve 1_{Hyll} for the lower nuclear charge ($Z^{\mathrm{eff}}_{\mathrm{P,T}} = 1.6875$, with screening in $\varphi_{i,f}$). This is explained by means of the mean radius $\bar{r}$ of an electron in e.g. the hydrogenic model for a fixed nuclear charge Z, with the principal n and orbital l quantum numbers:

$$\bar{r} \equiv \langle R_{nl}|r|R_{nl}\rangle = \frac{3n^2 - l(l+1)}{2Z}. \tag{3.4}$$

Here, the radial bound-state hydrogenlike wave function is denoted by R_{nl}. For e.g. the ground state ($n = 1$, $l = 0$), the relation (3.4) simplifies to $\bar{r} = 3/(2Z)$. This reciprocal relation between $\bar{r}$ and Z indicates the extent of compactness or diffuseness of the given orbital. The larger the Z, the smaller the $\bar{r}$. Stated equivalently, the radial orbitals with a larger Z are compact (compressed, more localized), whereas those with a smaller Z are diffused (less localized, more spread out).

This can be connected directly to the Heisenberg uncertainty principle for the two conjugate variables, the particle position in the configuration space and the particle momentum in the impulse space. Equivalently, the link can be stated on either the level of the probabilities or the probability amplitudes. The probability amplitudes are given by the pertinent wave functions in these two spaces. The probabilities are the squared absolute values of these probability amplitudes. Thus, the more the wave function is compact in the configuration space (the higher the Z, the lower the $\bar{r}$), the larger the momentum components of the corresponding function in the impulse space. Of course, the Fourier transform and its inverse map the given function from the configuration space to the impulse space and *vice versa*.

These features of atomic orbitals in the wave functions are of critical relevance to electron capture, especially at high energies. A fast moving projectile can capture one or more electrons from a target only if their orbital velocities are sufficiently high to match the large incident velocities. Therefore, this 'velocity matching' condition, involving the incident velocity and the electron velocity, would be more readily satisfied for the compact than for the diffused orbitals. In other words, the probability to capture electrons is higher for more compact than for more diffused orbitals (i.e. for the larger nuclear charges Z than for the smaller ones). Capture becomes non-negligible only when there is an appreciable overlap between the initial and final orbitals. At

high incident velocities, capture is favored by the large momentum components of the bound states projected on both the projectile and target waves.

Therefore, because it is more likely to capture one or two electrons by an alpha particle from a helium target with the unscreened ($Z_{\rm T} = 2$) than with the screened ($Z_{\rm T}^{\rm eff} = 1.6875$) nuclear charges in the ground-state wave functions, we have $Q_{\rm Hydr} > Q_{\rm Hyll}$, as seen in Fig. 3 from the curves $1_{\rm Hydr}$ and $1_{\rm Hyll}$, respectively. This occurs for both single and double capture, as is clear from the top and bottom graphs in this figure.

It should be re-stressed that $Q_{\rm Hydr}$ and $Q_{\rm Hyll}$ in the CDW-4B method for double capture are computed with the electronic full Coulomb wave functions centered on the unscreened nuclear charges ($Z_{\rm P,T} = 2$). This permits an unequivocal check of the sensitivity of total cross sections to the alteration of the nuclear charges $Z_{\rm P,T}$ solely in the one-parameter ground-state helium wave functions. If the nuclear charges $Z_{\rm P,T}$ were changed simultaneously in both the bound and continuum wave functions for double capture, the different effects stemming from these two functions would not be unambiguously separable.

Continuing further with the analysis, we shall concentrate only on double capture. The next theme to address is the role of screening of the bare nuclear charges $Z_{\rm P,T}$ also in the continuum states. One of the ways to investigate the screened continuum state is to place the Coulomb centers of distortions of the initial and final unperturbed states onto the effective nuclear charges $Z_{\rm P,T}^{\rm eff} = Z_{\rm T} - 5/16$. Such a prescription may amount to replacing the original problem (2.1) by the following effective problem:

$$Z_{\rm P}^{\rm eff} + (Z_{\rm T}^{\rm eff}; e_1, e_2)_i \longrightarrow (Z_{\rm P}^{\rm eff}; e_1, e_2)_f + Z_{\rm T}^{\rm eff}, \tag{3.5}$$

where $Z_{\rm P,T}^{\rm eff} = Z_{\rm P,T} - 5/16$ and $i = f = 1s^2$. For this problem too, the corresponding correct boundary conditions are satisfied in all the presently analyzed distorted wave methods. The one-parameter heliumlike ground-state wave functions of Hylleraas [27] with the damping factors $Z_{\rm P,T}^{\rm eff}$ in the exponentials are employed in process (3.5). The total Hamiltonian for process (3.5) does not contain the electron-electron Coulomb potential $1/r_{12}$. Therefore, there could be no further Slater screening of the already screened nuclear charges $Z_{\rm P,T}^{\rm eff}$, implying that process (3.5) is treated as an uncorrelated collision. To relate to the original problem (2.1), the bare nuclear charge $Z_{\rm P,T}$ in $Z_{\rm P,T}^{\rm eff} = Z_{\rm P,T} - 5/16$ from process (3.5) will now be specified as $Z_{\rm P,T} = 2$, so that hereafter we have $Z_{\rm P,T}^{\rm eff} = 1.6875$.

To avoid confusion, a clarification might be helpful here because of a twofold role of the Hylleraas wave function [27]. In processes (2.1) and (3.5), this one-parameter heliumlike wave function describes the correlated and uncorrelated model, depending on whether $1/r_{12}$ is retained or omitted in the search for the binding energy of the two-electron atomic system, respectively. In process (2.1), it is 'the hydrogenic model' that is uncorrelated ($1/r_{12} = 0$). On the other hand, 'the Hylleraas model' is uncorrelated in process (3.5) because therein we have $1/r_{12} = 0$.

The total cross sections from the CDW-4B method for processes (3.1) and (3.5) are displayed in Fig. 4 by the two curves, A and B, respectively. To re-emphasize, curves A and B are due to the same Hylleraas wave functions for the helium ground states in both channels. The difference is that curves A and B refer to $Z_{\rm P,T} = 2$ and

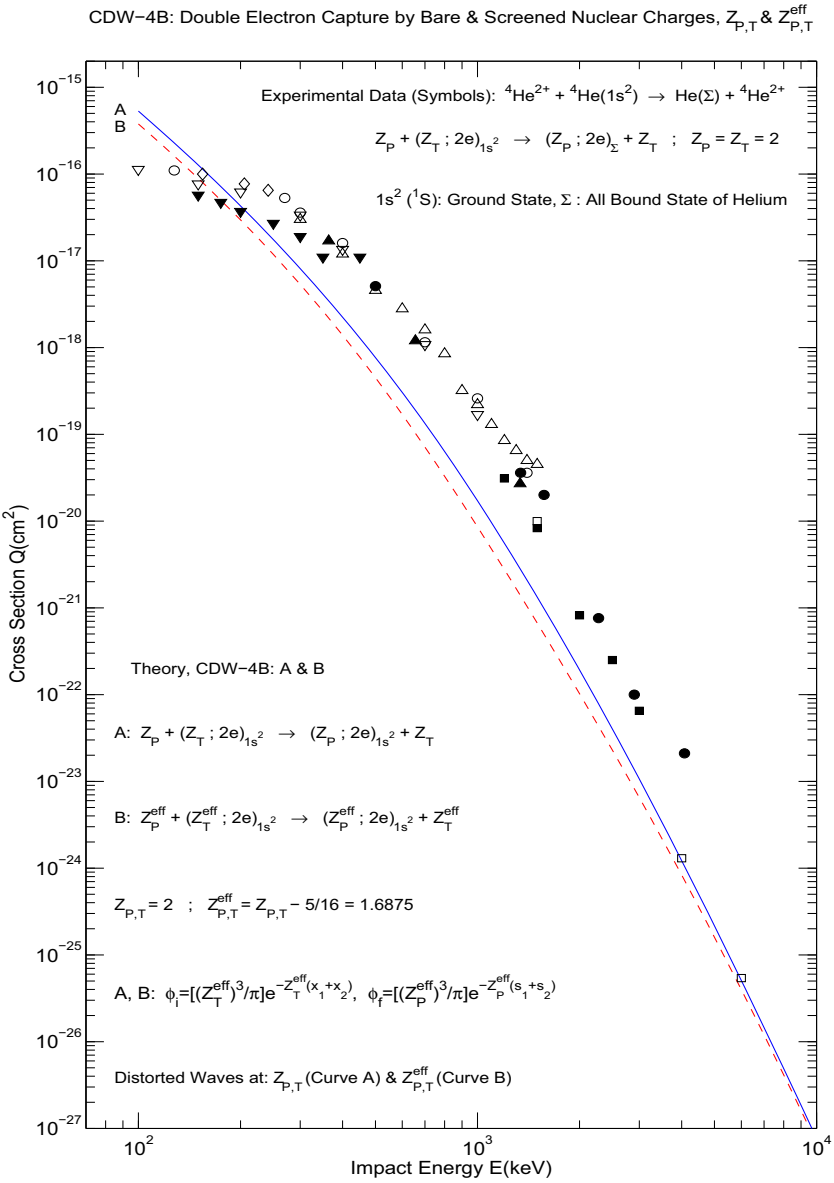

Fig. 4 Total cross sections $Q(\mathrm{cm}^2)$ as a function of impact energy $E(\mathrm{keV})$ for double capture in processes (3.1) and (3.2) in computations and measurements, respectively. Sensitivity of the results from the CDW-4B method relative to the screening of nuclear charges in the electronic full Coulomb wave functions. The ground-state wave function of Hylleraas [27] is employed with one parameter, $Z^{\mathrm{eff}}_{\mathrm{P,T}} = 1.6875$. The solid and dashed curves are for the unscreened and screened nuclear charges $Z_{\mathrm{P,T}} = 2$ and $Z^{\mathrm{eff}}_{\mathrm{P,T}} = 1.6875$ in the electronic full Coulomb wave functions, respectively. Experimental data for process (3.2): ▼ [18], ▲ [19], △ [20], ◇ [21], ○ [22], ▽ [23], ■ [24], □ [25] and ● [26]. For details, see the main text (color online)

$Z^{\text{eff}}_{\text{P,T}} = 1.6875$ for the unscreened and screened nuclear charges in the two electronic full Coulomb wave functions from the entrance and exit channels, respectively.

At all energies, Fig. 4 reveals a notable discrepancy between the results assigned to the unscreened (curve A) and screened (curve B) electronic full Coulomb wave functions. Specifically, below 3000 keV, curve B significantly underestimates curve A. Moreover, curve A itself is in large disagreement with most of the available experimental data shown in Fig. 4. This disagreement is further exacerbated with curve B. It can be concluded that at all the displayed energies in Fig. 4, the total cross sections in the CDW-4B method are very sensitive to the screening effect within the Coulomb wave functions of the initial and final two-electron continuum intermediate states.

Similar sensitivity tests are also made in the BCIS-4B and BDW-4B methods for processes (3.1) and (3.5). Both methods employ the same Hylleraas ground-state helium wave functions [27] with the common one-parameter $Z^{\text{eff}}_{\text{P,T}} = 1.6875$ appearing in the two-electron exponentials. They use the Coulomb distortions centered on $Z_{\text{P,T}} = 2$ and $Z^{\text{eff}}_{\text{P,T}} = 1.6875$ for (3.1) and (3.5), respectively. It is seen that the BCIS-4B (Fig. 5) and BDW-4B (Fig. 6) methods are much less sensitive than the CDW-4B method (Fig. 4) to the choice of the nuclear charges ($Z_{\text{P,T}} = 2$ or $Z^{\text{eff}}_{\text{P,T}} = 1.6875$) in the Coulomb distortions. More precisely, for either the BCIS-4B (Fig. 5) or BDW-4B (Fig. 6) methods, it is merely around the Massey peak (in the vicinity of about 100 keV) that there is at most a factor of 2 difference between the results for (3.1) and (3.5).

It is also of interest to plot together the curves from the BCIS-4B and BDW-4B methods for processes (3.1) and (3.5), as done in Figs. 7 and 8, respectively. Regarding process (3.1), with $Z^{\text{eff}}_{\text{P,T}} = 1.6875$ in the bound states and $Z_{\text{P,T}} = 2$ in the continuum states, Fig. 7 shows that the curves for the cross sections in the BCIS-4B and BDW-4B methods lie quite close to each other. However, as to process (3.5), with $Z^{\text{eff}}_{\text{P,T}} = 1.6875$ in both the bound and continuum states, the curves from the BCIS-4B and BDW-4B methods in Fig. 8 coincide exactly with each other, as they should.

To explain this coincidence, it is recalled that for rearrangement collisions, the two different perturbation potentials in the given transition amplitude are defined by applying the operator $H - E$ to the initial χ_i^+ and to the final χ_f^- distorted wave functions. Here, H and E are the total Hamiltonian operator and energy of the whole system. Let then the initial χ_i^+ and final χ_f^- distorted waves be taken from the CB1-4B and CDW-4B methods for double capture, respectively. By applying the $H - E$ operator to χ_i^+ and χ_f^-, the two transition amplitudes would be formulated, the former in the BCIS-4B method and the latter in the BDW-4B method.

The obtained transition amplitudes from the BCIS-4B and BDW-4B methods would be identical if the exact bound-state wave functions $\varphi_{i,f}$ were known. However, if these are unavailable (as is actually the case for heliumlike atoms or ions), any approximate wave functions $\varphi_{i,f}$ would yield two different transition amplitudes. On the level of the corresponding total cross sections, such differences between the BCIS-4B and BDW-4B methods are seen in Fig. 7. In Fig. 7, the inter-electron potential $1/r_{12}$ is not set equal to zero. Rather, as mentioned earlier, this electron-electron repulsive potential is a part of the Hylleraas minimization procedure of the expectation value of the exact total two-electron Hamiltonian, which includes $1/r_{12}$.

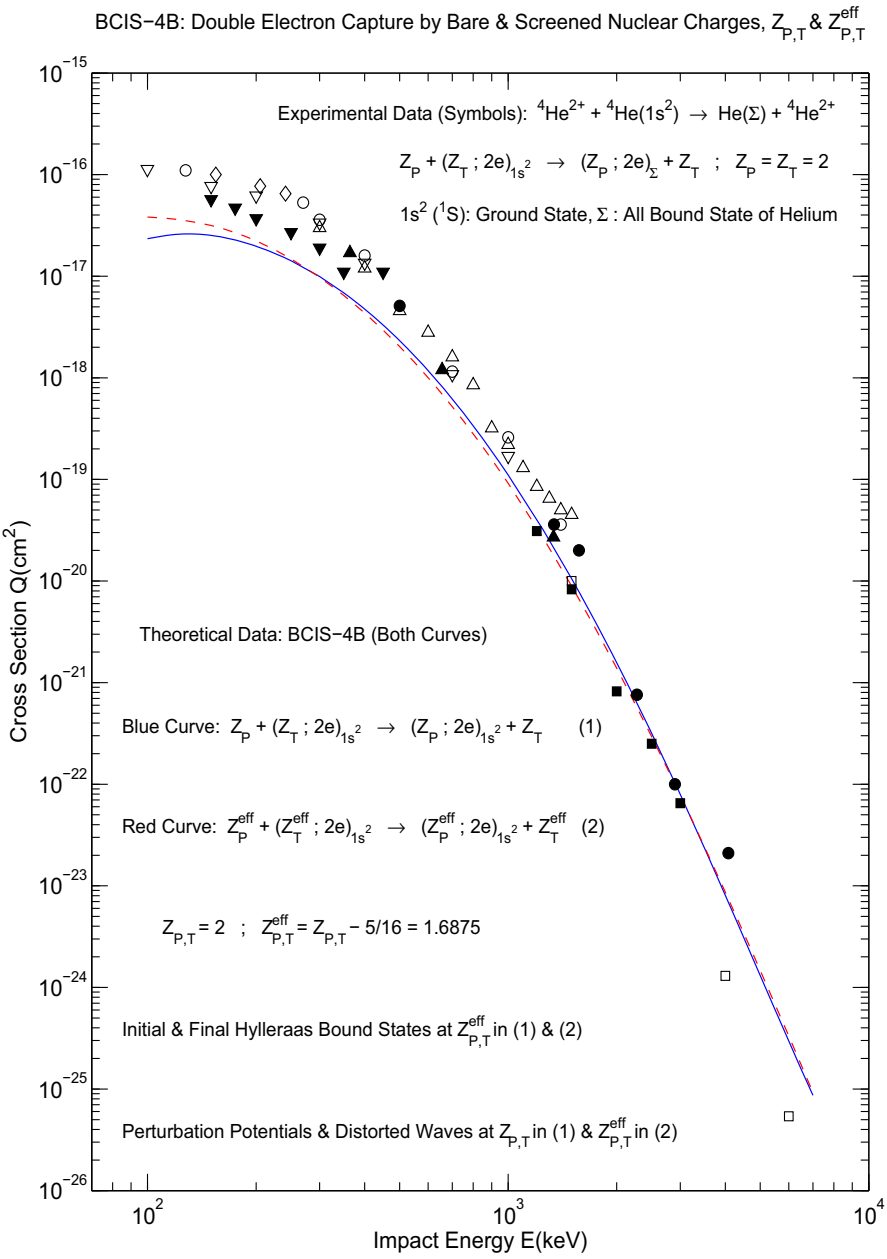

Fig. 5 Total cross sections $Q(\mathrm{cm}^2)$ as a function of impact energy $E(\mathrm{keV})$ for double capture in processes (3.1) and (3.2) in computations and measurements, respectively. Sensitivity of the results from the BCIS-4B method relative to the screening of nuclear charges in the Coulomb distorting factors. The ground-state wave function of Hylleraas [27] is employed with one parameter, $Z^{\mathrm{eff}}_{\mathrm{P,T}} = 1.6875$. The solid and dashed curve are for the unscreened and screened nuclear charges $Z_{\mathrm{P,T}} = 2$ and $Z^{\mathrm{eff}}_{\mathrm{P,T}} = 1.6875$ in the Coulomb distorting factors, respectively. Experimental data for process (3.2): ▼ [18], ▲ [19], △ [20], ◇ [21], ○ [22], ▽ [23], ■ [24], □ [25] and ● [26]. For details, see the main text (color online)

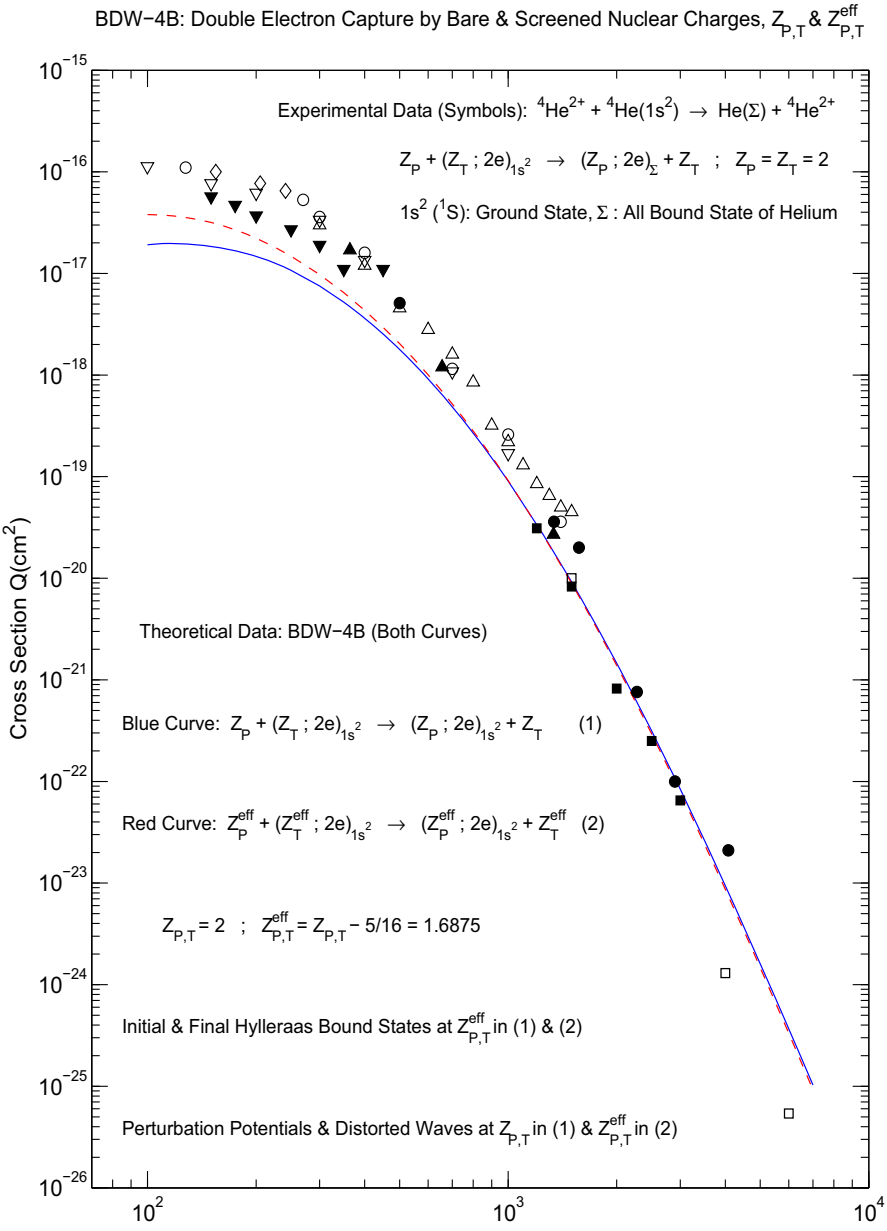

Fig. 6 Total cross sections $Q(\mathrm{cm}^2)$ as a function of impact energy $E(\mathrm{keV})$ for double capture in processes (3.1) and (3.2) in computations and measurements, respectively. Sensitivity of the results from the BDW-4B method relative to the screening of nuclear charges in the Coulomb distorting factors. The ground-state wave function of Hylleraas [27] is employed with one parameter, $Z^{\mathrm{eff}}_{\mathrm{P,T}} = 1.6875$. The solid and dashed curve are for the unscreened and screened nuclear charges $Z_{\mathrm{P,T}} = 2$ and $Z^{\mathrm{eff}}_{\mathrm{P,T}} = 1.6875$ in the Coulomb distorting factors, respectively. Experimental data for process (3.2): ▼ [18], ▲ [19], △ [20], ◇ [21], ○ [22], ▽ [23], ■ [24], □ [25] and ● [26]. For details, see the main text (color online)

However, for process (3.5), using $Z_{\mathrm{P,T}}^{\mathrm{eff}} = 1.6875$ in the initial and final bound and continuum states, the one-parameter Hylleraas wave functions $\varphi_{i,f}$ are, in fact, the exact ground-state helium wave functions for this completely uncorrelated model (where $1/r_{12} = 0$ throughout). In such a case, the expressions for the transition amplitudes would be the same irrespective of whether the operator $H - E$ is applied to the initial χ_i^+ or to the final χ_f^- scattering states. This is why in Fig. 8, the two curves from the ensuing theories, the BCIS-4B and BDW-4B methods, are seen to be coincident.

The main focus in Figs. 4-6 is on the sensitivity of total cross sections with respect to the screening effect in the Coulomb distortions of the initial and final unperturbed scattering states in the CDW-4B, BCIS-4B and BDW-4B methods. This is carried out by considering one method at a time. Thus, Fig. 4 is for the CDW-4B, Fig. 5 for the BCIS-4B and Fig. 6 for the BDW-4B methods. These methods differ in the choices of the distorted waves in the total scattering wave functions.

For various practical applications, it is important to establish the relative sensitivity of total cross sections to the choice of Coulomb distortions when two or more distorted wave methods are compared. Such a testing is already performed in Figs. 7 and 8 where the BCIS-4B and BDW-4B methods are compared. A relatively mild difference is seen in Fig. 7 between these two methods for process (3.1) with the unscreened Coulomb distortions. On the other hand, for process (3.5), with the screened Coulomb distortions, the BCIS-4B and BDW-4B methods give the identical cross sections for the explained reason.

In the CB1-4B method, there are no electronic distorted wave functions at all. Instead, the initial and final unperturbed states are modified by the Coulomb distortions (the logarithmic phase factors) that describe the relative motion of heavy scattering aggregates. Even such phases are completely absent from the symmetric collisions such as (3.1) or (3.2). In the BCIS-4B and BDW-4B methods, both the Coulomb logarithmic phases for heavy nuclei and the electronic full Coulomb wave functions are always present, including the homo- and hetero-nuclear cases of process (2.1), i.e. for $Z_{\mathrm{P}} = Z_{\mathrm{T}}$ and $Z_{\mathrm{P}} \neq Z_{\mathrm{T}}$, respectively.

Regarding the first- and second-order theories, the most relevant is to compare the CB1-4B and BCIS-4B methods. They share the same perturbation interactions (three electrostatic Coulomb potentials). Moreover, they have the same total scattering wave functions in one channel, but differ in the other channel. Only the BCIS-4B method contains the electronic distortions (two full Coulomb wave functions in one channel). Thus, the relative performance of the CB1-4B and BCIS-4B methods with respect to the corresponding measurements would inform about the role of the continuum intermediate states of two electrons in double capture [9].

Figure 9 shows that the CB1-4B method [5, 6] is in very good agreement with measurements at 175-800 keV. However, at 900-3000 keV, the CB1-4B method overestimates the experimental data from Refs. [18–26] by a factor varying from 3 to about 10. This factor increases to about 20 relative to the measurements from Ref. [25] at higher energies. However, the only two experimental data points near 4000 keV [25, 26] are controversial as they are themselves in a very large mutual disparity (within a factor of 20).

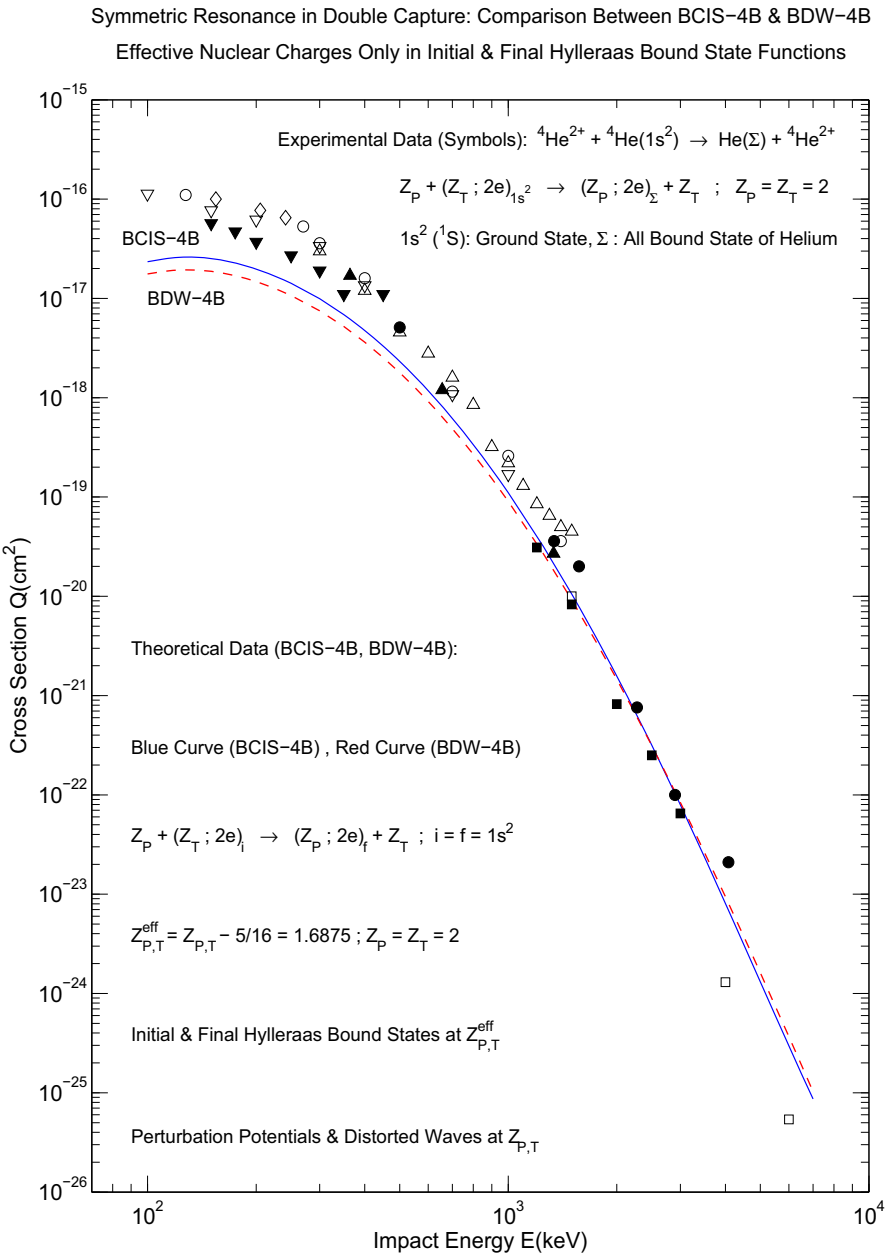

Fig. 7 Total cross sections $Q(\mathrm{cm}^2)$ as a function of impact energy $E(\mathrm{keV})$ for double capture in processes (3.1) and (3.2) in computations and measurements, respectively. Sensitivity of the results relative to the choice of distorted waves and perturbation potentials in the BCIS-4B and BDW-4B methods. Both methods employ the same ground-state wave function of Hylleraas [27] with one parameter, $Z^{\mathrm{eff}}_{\mathrm{P,T}} = 1.6875$. Moreover, the unscreened nuclear charges $Z_{\mathrm{P,T}} = 2$ are used in both methods for the distorted wave and perturbation potentials. Experimental data for process (3.2): ▼ [18], ▲ [19], △ [20], ◇ [21], ○ [22], ▽ [23], ■ [24], □ [25] and • [26]. For details, see the main text (color online)

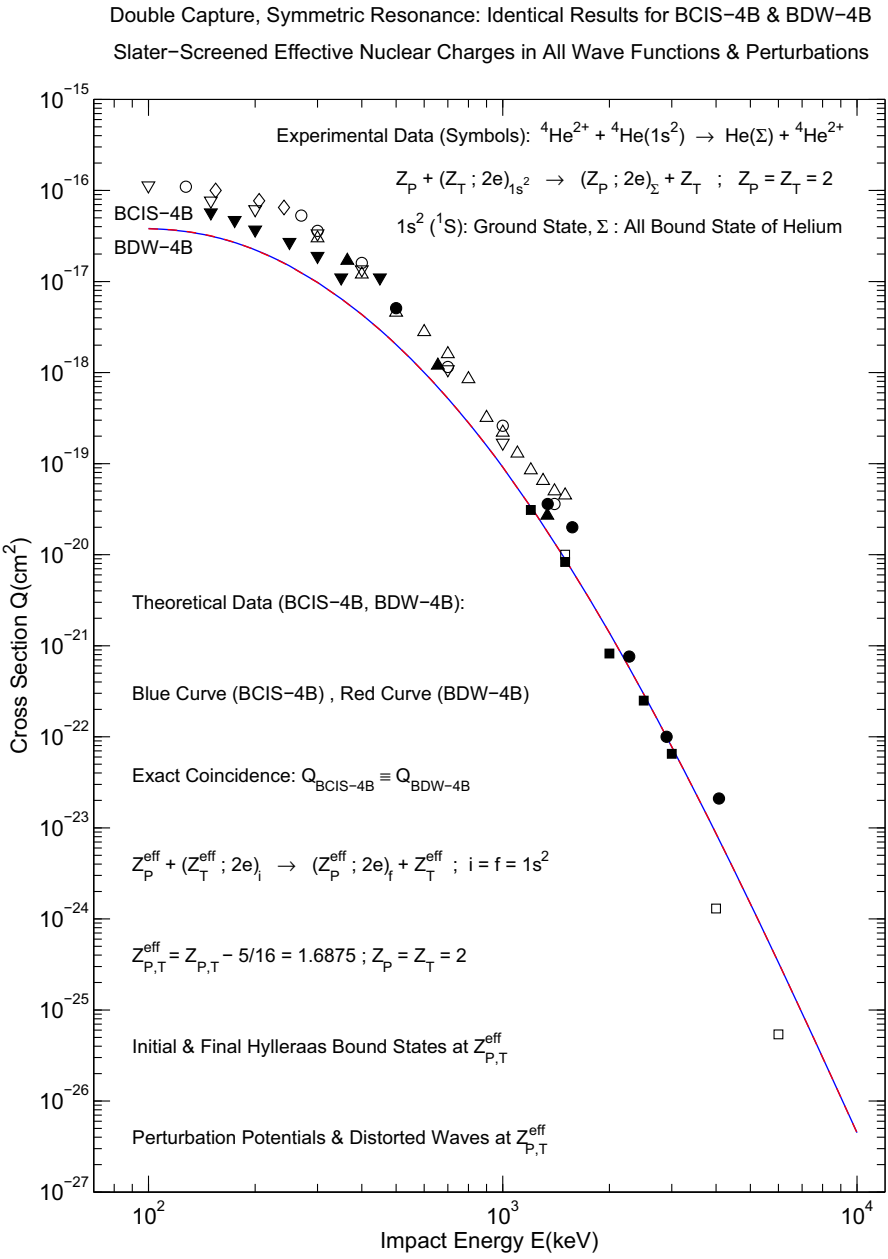

Fig. 8 Total cross sections $Q(\text{cm}^2)$ as a function of impact energy $E(\text{keV})$ for double capture in processes (3.5) and (3.2) in computations and measurements, respectively. Sensitivity of the results relative to the choice of distorted waves and perturbation potentials in the BCIS-4B and BDW-4B methods. Both methods employ the same ground-state wave function of Hylleraas [27] with one parameter, $Z_{P,T}^{\text{eff}} = 1.6875$. Moreover, the screened nuclear charges $Z_{P,T}^{\text{eff}} = 1.6875$ are used in both methods for the distorted wave and perturbation potentials. Experimental data for process (3.2): ▼ [18], ▲ [19], △ [20], ◇ [21], ○ [22], ▽ [23], ■ [24], □ [25] and ● [26]. For details, see the main text (color online)

Conversely, below about 600 keV, the BCIS-4B method [9] underestimates the measurements, within a factor of at most 5. At 900-4000 keV, the BCIS-4B method is in excellent agreement with the experimental data from Refs.[19–26]. The discrepancy between the CB1-4B and BCIS-4B methods increases with augmentation of the impact energy. Thus, the ratios of the cross sections from the CB1-4B and BCIS-4B methods are about 15 and 112 at 100 and 8000 keV, respectively. Such a striking difference runs contrary to good agreement between these two methods for single capture at intermediate and high energies [16]. It can then be stated, that the electronic continuum intermediate states in the BCIS-4B method (second-order) are of critical importance for double capture compared to the CB1-4B method (first-order), particularly at high energies.

Figure 10 compares the three methods that have the identical perturbation potentials and the final total scattering wave function χ_f^- from the exit channel. These methods differ in the initial total scattering wave functions from the entrance channel. We are referring here to the CDW-4B, CDW-EIS-4B and BDW-4B methods. They are seen in Fig. 10 to yield strikingly different total cross sections. The unsatisfactory status of the CDW-4B method relative to the measurements is already discussed with Fig. 4. The best agreement with the most experimental data is obtained with the BDW-4B method.

On the other hand, Fig. 10 shows that the CDW-EIS-4B method fails dramatically below 1000 keV as it underestimates the experimental data by three orders of magnitude. Surprisingly, such a complete breakdown of this method occurs well within its expected main validity domain.

Moreover, the CDW-EIS-4B method underestimates the CDW-4B method in Fig. 10 also by huge factors, ranging from 20 to 4000 at the impact energies decreased from 1000 to 100 keV, respectively. The enormous difference between the total cross sections from the CDW-4B and CDW-EIS-4B methods proves that the electronic eikonalization of the two full Coulomb wave functions in the latter theory is utterly inadequate. An alternative is to use the eikonalization of the Coulomb distortions due to the relative motions of heavy particles. This is done in the BDW-4B method which, as a consequence, largely outperforms the CDW-EIS-4B method in comparison with the experimental data on double capture.

The discussed multiplicative effect is maximal in the CDW-4B method by the product of two electronic continuum wave functions in each channel. The underlying double scattering mechanism might be over-expressed (too demanding) and could lower the probability for simultaneous capture of two electrons. This might be one of the reasons for which the CDW-4B method severely underestimates the experimental data at most energies. On the other hand, restricting the multiplicative effect by having the product of two electronic continuum wave functions only one channel, the BCIS-4B and BDW-4B methods yield much better agreement with the measurements than the CDW-4B method.

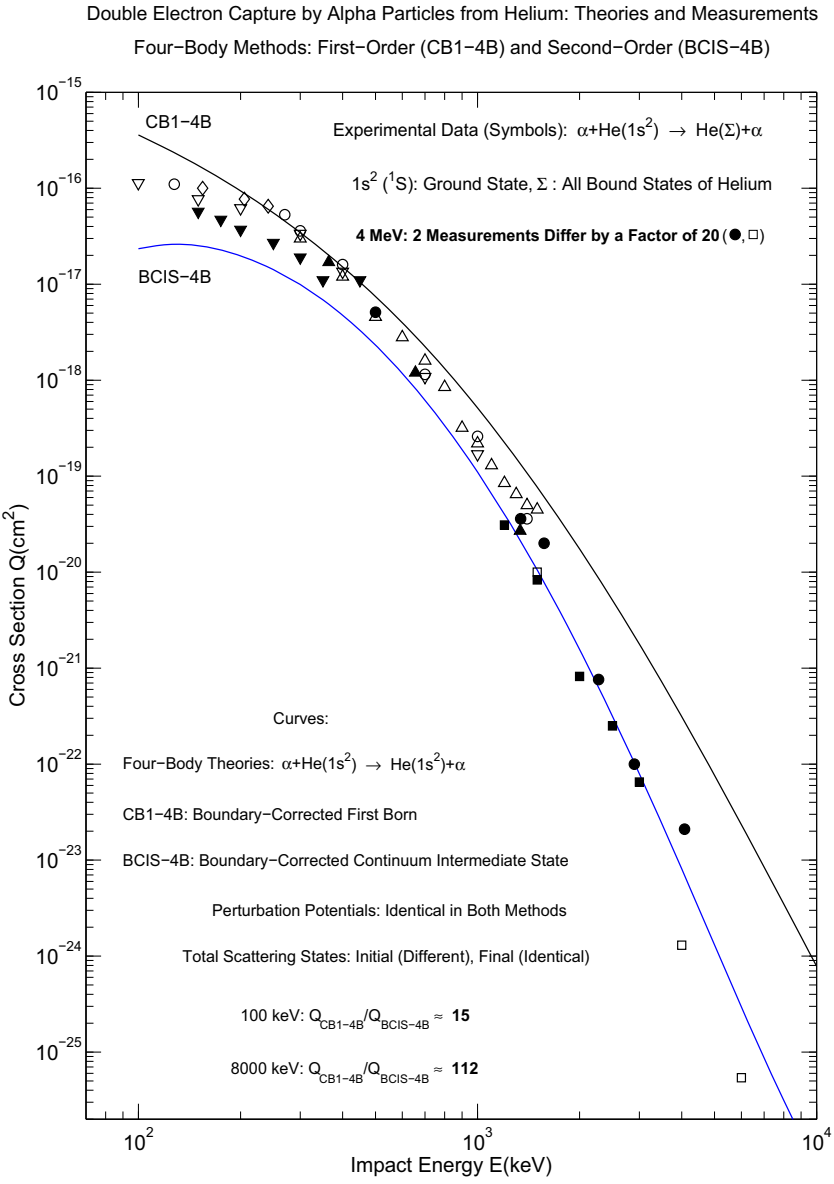

Fig. 9 Total cross sections $Q(\mathrm{cm}^2)$ as a function of impact energy $E(\mathrm{keV})$ for double capture in processes (3.1) and (3.2) in computations and measurements, respectively. Sensitivity of the results relative to the choice of distorted waves and perturbation potentials in the CB1-4B and BCIS-4B methods. Both methods employ the same ground-state wave function of Hylleraas [27] with one parameter, $Z_{\mathrm{P,T}}^{\mathrm{eff}} = 1.6875$. There are no Coulomb distortions in the CB1-4B method for symmetric double capture in process (3.1). The unscreened nuclear charges $Z_{\mathrm{P,T}} = 2$ are used in the BCIS-4B method for the distorted wave and perturbation potential. Experimental data for process (3.2): ▼ [18], ▲ [19], △ [20], ◇ [21], ○ [22], ▽ [23], ■ [24], □ [25] and ● [26]. For details, see the main text (color online)

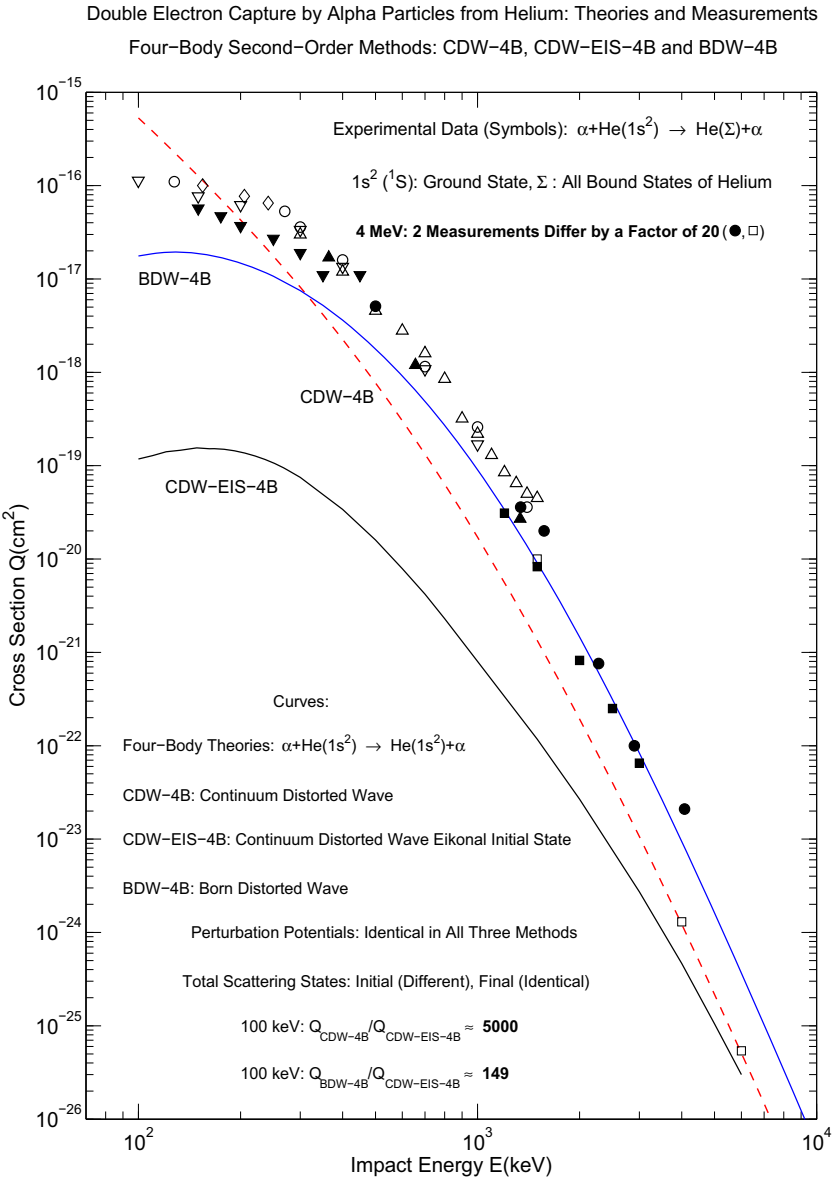

Fig. 10 Total cross sections $Q(\mathrm{cm}^2)$ as a function of impact energy $E(\mathrm{keV})$ for double capture in processes (3.1) and (3.2) in computations and measurements, respectively. Sensitivity of the results relative to the choice of distorted waves and perturbation potentials in the CDW-4B, CDW-EIS-4B and BDW-4B methods. All the three methods employ the same ground-state wave function of Hylleraas [27] with one parameter, $Z_{\mathrm{P,T}}^{\mathrm{eff}} = 1.6875$. They have the identical solution for the distorted wave problem in the exit channel, but differ in the entrance channel. The unscreened nuclear charges $Z_{\mathrm{P,T}} = 2$ are used for the distorted wave problems in all the three methods. Experimental data for process (3.2): ▼ [18], ▲ [19], △ [20], ◇ [21], ○ [22], ▽ [23], ■ [24], □ [25] and ● [26]. For details, see the main text (color online)

4 Discussion and conclusions

We carried out a comparative analysis of several of the frequently applied four-body quantum-mechanical distorted wave methods with the correct Coulomb boundary conditions for two-electron transfer in ion-atom collisions. Use is made of the newly performed computations on total cross sections at intermediate and high impact energies (100-10000 keV). The heliumlike targets (of nuclear charge Z_T) are taken to be impacted by heavy nuclei (of charge Z_P and velocity $\boldsymbol{v}$). In the illustrations, double electron capture from helium by alpha particles is exemplified by comparing different theories with measurements.

The influence of the Slater electronic screening of the nuclear charges in the bound and continuum wave functions is examined within the three second-order theories in their four-body versions, the continuum distorted wave (CDW-4B), the boundary-corrected continuum intermediate state (BCIS-4B) and the Born distorted wave (BDW-4B) methods. At all the considered energies, the most pronounced differences between the total cross sections with the bare and screened (effective) nuclear charges are found in the CDW-4B method. By comparison, no appreciable sensitivity is detected in the BCIS-4B and BDW-4B methods above about 200 and 300 keV, respectively. Moreover, the total cross sections in the BCIS-4B and BDW-4B methods are everywhere close to each other when using the screened bound states and the Coulomb distorted wave functions with the bare nuclear charges. In the case when the same Slater-screened nuclear charges are employed in the bound and continuum states, the computed total cross sections in the BCIS-4B and BDW-4B methods coincide with each other exactly, as expected.

Also investigated is the relative sensitivity of total cross sections to eikonalizations of the full Coulomb continuum wave functions for motions of electrons and heavy particles. Moreover, the repercussions of different choices of distorted waves are analyzed. Of particular interest is to juxtapose the three second-order theories that share the same perturbation potentials and the total scattering wave functions in the exit channel, but differ in their descriptions of the entrance channel. These are the CDW-4B, BDW-4B and the four-body continuum distorted wave - eikonal initial state (CDW-EIS-4B) methods. Regarding the internuclear potential $V_{PT} = Z_P Z_T / R$, the CDW-4B, BDW-4B and CDW-EIS-4B methods contain the same product of the initial and final (complex conjugated) Coulomb logarithmic phase factors for the relative motion of the two heavy nuclei in the entrance and exit channels, respectively.

In the heavy mass unit, this product is reduced to a lone phase, which can be omitted since it does not contribute to any total cross section. The underlying mechanism, yielding the internuclear phase, is eikonalization of the full Coulomb wave function for V_{PT}. Such a Coulomb wave can safely be replaced by its leading asymptotic term (the logarithmic phase factor) with a negligible error, which is smaller than or equal to the reciprocal of the large reduced mass of the two heavy nuclei.

Further, the CDW-4B, BDW-4B and CDW-EIS-4B methods possess the identical product of the two full electronic Coulomb wave functions for the final states. After the said elimination of the internuclear phase from the transition amplitude for computations of total cross sections, it makes interesting reading to peer into the structure of the distorted waves for the initial state in these three methods. In the entrance channel, the

CDW-4B method has the product of the two full electronic Coulomb wave functions (of variables $\boldsymbol{s}_1$ and $\boldsymbol{s}_2$) centered on Z_P. This product is replaced by its asymptotic form $[(vs_1 + \boldsymbol{v}\cdot\boldsymbol{s}_1)(vs_2 + \boldsymbol{v}\cdot\boldsymbol{s}_2)]^{-iZ_P/v}$ in the CDW-EIS-4B method. The latter compound eikonal initial phase (being a valid representation of the associated full Coulomb state only at large distances) is asymptotically equivalent to $(vR - \boldsymbol{v}\cdot\boldsymbol{R})^{-2iZ_P/v}$, which is employed in the BDW-4B method.

It is precisely this equivalence that is crucial for establishing the correct asymptotic behaviors of the total scattering states in the entrance channel. However, the transition amplitudes integrate these eikonal phases (alongside the other integrands) over all the distances in a multi-dimensional configuration space of the four interacting particles. Moreover, the main contributions to these integrals stem from short distances dictated by the exponentially attenuated atomic bound-state wave functions. Therefore, while the eikonal phases $[(vs_1 + \boldsymbol{v}\cdot\boldsymbol{s}_1)(vs_2 + \boldsymbol{v}\cdot\boldsymbol{s}_2)]^{-iZ_P/v}$ and $(vR - \boldsymbol{v}\cdot\boldsymbol{R})^{-2iZ_P/v}$ are asymptotically equivalent outside the transition amplitudes, they can still give different contributions to the computed total cross sections. Such differences, embodied in the CDW-EIS-4B and BDW-4B methods, are enormous for double capture.

At all the presently considered energies, there exists a strong sensitivity of the computed total cross sections to the choice of the distorted wave functions in double capture. In particular, the CDW-EIS-4B method fails flagrantly at all the studied energies. It hugely underestimates the CDW-4B method and all the available experimental data by an astonishing factor ranging from 1 to 3 orders of magnitude below 1000 keV. This completely invalidates the procedure of eikonalization of the product of the two electronic Coulomb continuum wave functions in double capture.

On the other hand, the BDW-4B method largely outperforms both the CDW-4B and CDW-EIS-4B methods by yielding the total cross sections in a reasonable proximity of the majority of the existing experimental data in the keV-MeV region, starting already from about 180 keV. This proves that eikonalization of the full Coulomb wave functions for the relative motion of heavy particles in the BCIS-4B and BDW-4B methods for double capture is physically by far more adequate than the usage of the electronic eikonal phases in the CDW-EIS-4B method. Partly, it is the 'multiplicative effect' in the entrance channel (the product of two eikonal electronic phases) that has a deleterious impact on the performance of the CDW-EIS-4B method for double capture. The same method with only one eikonal electronic phase for single capture is in excellent accord with the corresponding measurements.

Regarding the experimental data available for two-electron transfer from helium by alpha particles, various measurements are also quite dispersed. For instance, the most pronounced disagreement (within a factor of 20) is at 4000 keV between the total cross sections measured by Schuch *et al* [25] and Afrosimov *et al* [26]. Moreover, above 1500 keV, even the energy behaviors of total cross sections for double capture vary from one measurement to another.

In particular, the measured cross sections of Schuch *et al* [25] for their reported two data points (4000, 6000 keV) are completely out of the trend with the experimental data from the other measurements. Such a sharply conflicting circumstance particularly above 1000 keV does not permit a reasonably realistic assessment of the relative performance of different high-energy theoretical methods. Evidently, for the total cross sections under the present study (and beyond), it would be desirable to refresh the only

existing high-energy measurement database from 1962-1993. Some new experimental data on total cross sections are much needed to clarify the confusing situation for a process as fundamental as double capture from helium targets by alpha particles.

Acknowledgements This work is supported by the research grants from Radiumhemmet at the Karolinska University Hospital and the City Council of Stockholm (FoUU) to which the author is grateful. Open Access has been provided by the Karolinska Institute, Stockholm, Sweden.

Author Contributions The entire work from the design to its completion has been carried out by the author himself.

Funding This work is funded by Radiumhemmet at the Karolinska University Hospital and the City Council of Stockholm. Open access funding provided by Karolinska Institute.

Availability of data and materials Data from this work can be available to other researchers in this field upon request to the author.

Declarations

Competing interests The author has no competing interests.

Ethical approval Not applicable.

References

1. Dž. Belkić, Review of theories on double electron capture in fast ion-atom collisions. J. Math. Chem **47**, 1420–1467 (2010)
2. Dž. Belkić, Double charge exchange in ion-atom collisions using distorted wave theories with two-electron continuum intermediate states in one or both scattering channels. J. Math. Chem. **57**, 1–58 (2019)
3. Dž. Belkić, Total cross sections in five methods for two-electron capture by alpha particles from helium: CDW-4B, BDW-4B, BCIS-4B, CDW-EIS-4B and CB1-4B. J. Math. Chem. **58**, 1133–1176 (2020)
4. Dž. Belkić, R. Gayet, A. Salin, Electron capture in high-energy ion-atom collisions. Phys. Rep. **56**, 279–369 (1979)
5. Dž. Belkić, Symmetric double charge exchange in fast collisions of bare nuclei with helium-like atomic systems. Phys. Rev. A **47**, 189–200 (1993)
6. Dž. Belkić, Two-electron capture from helium-like atomic systems by completely stripped projectiles. J. Phys. B **26**, 497–508 (1993)
7. Dž. Belkić, I. Mančev, Formation of H^- by double charge exchange in fast proton-helium collisions. Phys. Scr. **45**, 35–42 (1992)
8. Dž. Belkić, I. Mančev, Four-body CDW approximation: dependence of prior and post total cross sections for double charge exchange upon bound-state wave-functions. Phys. Scr. **46**, 18–23 (1993)
9. Dž. Belkić, Importance of intermediate ionization continua for double charge exchange at high energies. Phys. Rev. A **47**, 3824–3844 (1993)

10. Dž. Belkić, Double charge exchange at high impact energies. Nucl. Instrum. Methods Phys. Res. B **86**, 62–81 (1994)
11. Dž. Belkić, I. Mančev, M. Mudrinić, Two-electron capture from helium by fast alpha particles. Phys. Rev. A **49**, 3646–3658 (1994)
12. A.E. Martínez, R.D. Rivarola, R. Gayet, J. Hanssen, Double electron capture theories: Second order contributions. Phys. Scr. **T80**, 124–127 (1999)
13. Dž. Belkić, S. Saini, H. Taylor, A critical test of first-order theories for electron transfer in collisions between multicharged ions and atomic hydrogen. Phys. Rev. A **36**, 1601–1617 (1987)
14. Dž. Belkić, H. Taylor, First-order theory for charge exchange with correct boundary conditions: General results for hydrogenlike and multielectron targets. Rev. A **36**, 1991–2006 (1987)
15. Dž. Belkić, *Principles of Quantum Scattering Theory* (Institute of Physics, Bristol, 2004)
16. Dž. Belkić, *Quantum Theory of High-Energy Ion-Atom Collisions* (Taylor & Francis, London 2008)
17. Dž. Belkić, I. Mančev, J. Hanssen, Four-body methods for ion-atom collisions. Rev. Mod. Phys. **80**, 249–314 (2008)
18. S.K. Allison, Experimental results on charge-changing collisions of hydrogen and helium atoms and ions at kinetic energies above 0.2 keV. Rev. Mod. Phys. **30**, 1137–1168 (1958)
19. V.S. Nikolaev, L.N. Fateeva, I.S. Dmitriev, Ya.A. Teplova, Capture of several electrons by fast multicharged ions. J. Exp. Theor. Phys. **14**, 67–74 (1962) [Zh. Eksp. Teor. Fiz. **41**, 89–99 (1961)]
20. L.I. Pivovar, M.T. Novikov, V.M. Tubaev, Electron capture by helium ions in various gases in the 300–1500 keV energy range. J. Exp. Theor. Phys. **15**, 1035–1039 (1962) [Zh. Eksp. Teor. Fiz. **42**, 1490–1494 (1962)]
21. K.H. Berkner, R.V. Pyle, J.W. Stearns, J.C. Warren, Single- and double-electron capture by 7.2 to 181 keV $^3He^{++}$ ions in He. Phys. Rev. **166**, 44–46 (1968)
22. E.W. McDaniel, M.R. Flannery, H.W. Ellis, F.L. Eisele, W. Pope, *US Army Missile Research and Development Command*, Technical Report, No. H-78-1 (1977). https://www.army.mil/article/119547/research_center_paved_way_for_development
23. R.D. DuBois, Ionization and charge transfer in He^{2+}−rare gas collisions: II. Phys. Rev. A **36**, 2585–2593 (1987)
24. N.V. de Castro Faria, F.L. Freire Jr., A.G. de Pinho, Electron loss and capture by fast helium ions in noble gases. Phys. Rev. A **37**, 280–283 (1988)
25. R. Schuch, E. Justiniano, H. Vogt, G. Deco, N. Grün, Double electron capture by He^{2+} from He at high velocity. J. Phys. B **24**, L133–L138 (1991)
26. V.V. Afrosimov, D.F. Barash, A.A. Basalaev, N.A. Gushchina, K.O. Lozhkin, V.K. Nikulin, M.N. Panov, I.Y. Stepanov, Single- and double-electron capture from many-electron atoms by α particles in the MeV energy range. J. Exp. Theor. Phys. **77**, 554–561 (1993) [Zh. Eksp. Teor. Fiz. **104**, 3297–3310 (1993)]
27. E.A. Hylleraas, Neue Berechtnung der Energie des Heliums im Grundzustande, sowie tiefsten Terms von Ortho-Helium. Z. Phys. **54**, 347–366 (1929)
28. J. Silverman, O. Platas, F.A. Matsen, Simple configuration-interaction wave functions. I. Two-electron ions: A numerical study. J. Chem. Phys. **32**, 1402–1406 (1960)
29. L.C. Green, M.M. Mulder, M.N. Lewis, J.W. Woll Jr., A discussion of analytic and Hartree-Fock wave functions for $1s^2$ configurations from H^- to C. Phys. Rev. **93**, 757–761 (1954)
30. P.-O. Löwdin, Studies of atomic self-consistent fields. I. Calculation of Slater functions. Phys. Rev. **90**, 120–125 (1953)
31. Dž. Belkić, R. Gayet, Charge exchange in fast collisions of H^+ and He^{2+} with helium. J. Phys. B **10**, 1923–1932 (1977)